Cell Reports

Article

Phage biocontrol reduces the disease burden and modulates plant immunity through suppression of bacterial virulence

Graphical abstract

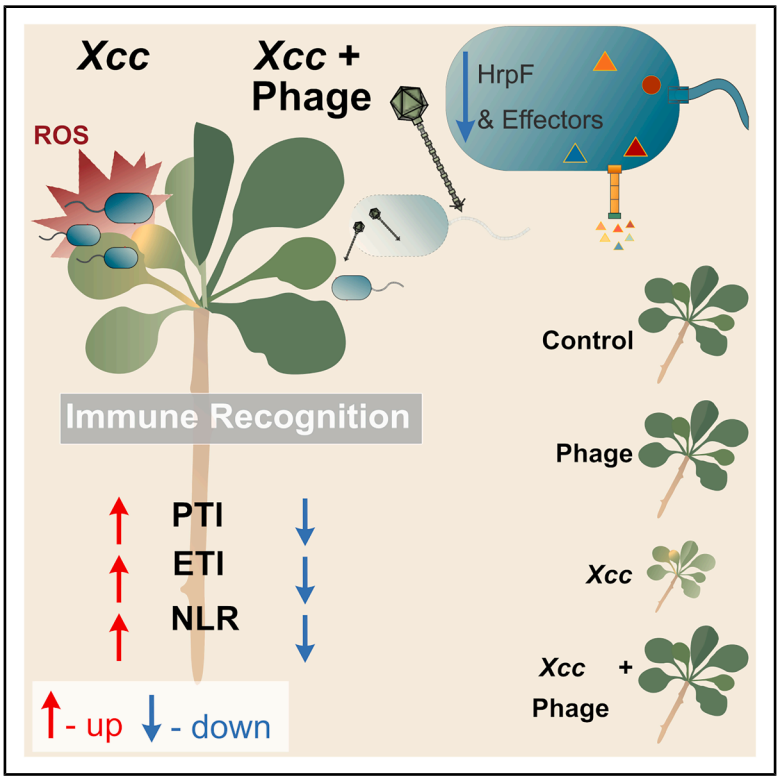

Authors

Sebastian H. Erdrich, Mirco T. Keilhammer, Swati Sharma, ..., Guido Grossmann, Julia Frunzke, Borjana Arsova

Correspondence

j.frunzke@fz-juelich.de (J.F.), b.arsova@fz-juelich.de (B.A.)

In brief

Erdrich et al. investigated the molecular interplay underlying bacteriophage-based biocontrol, using natural bacterial viruses for plant protection. They uncovered that phage-treated plants maintain biomass production comparable to uninfected controls while displaying an attenuated immune response. The bacterial pathogen showed reduced virulence-associated gene expression under phage pressure.

Highlights

- Phage-based biocontrol restores plant growth during *Xanthomonas* infection
- Phage treatment lowers, but does not eradicate, *Xanthomonas* loads
- Parallel transcriptomics reveals reduced plant immunity and bacterial virulence
- *Xanthomonas* has decreased resistance development against the phage, *in planta*

Erdrich et al., 2026, Cell Reports *45*, 117622
July 28, 2026
https://doi.org/10.1016/j.celrep.2026.117622

CellPress

Cell Reports

CellPress
OPEN ACCESS

Article

Phage biocontrol reduces the disease burden and modulates plant immunity through suppression of bacterial virulence

Sebastian H. Erdrich,[1,2,3,4] Mirco T. Keilhammer,[2,3,4] Swati Sharma,[1,2] Milan Župunski,[3] Ulrich Schurr,[1] Guido Grossmann,[3,5] Julia Frunzke,[2,4,*] and Borjana Arsova[1,6,*]

[1]Institute of Bio- and Geosciences, Department for Plant Sciences (IBG-2), Forschungszentrum Jülich, Jülich, Germany
[2]Institute of Bio- and Geosciences, Department for Biotechnology (IBG-1), Forschungszentrum Jülich, Jülich, Germany
[3]Institute of Cell and Interaction Biology (ICIB), Heinrich-Heine-University Düsseldorf, Düsseldorf, Germany
[4]Institute of Microbial Interactions, Heinrich-Heine-University Düsseldorf, Düsseldorf, Germany
[5]CEPLAS Cluster of Excellence on Plant Sciences, Heinrich-Heine-Universität Düsseldorf, Düsseldorf 40225, Germany
[6]Lead contact
*Correspondence: j.frunzke@fz-juelich.de (J.F.), b.arsova@fz-juelich.de (B.A.)
https://doi.org/10.1016/j.celrep.2026.117622

SUMMARY

Bacteriophages are emerging as modulators of plant-microbe interactions and promising biocontrol agents against bacterial plant pathogens. In this study, we investigate the tripartite interaction between *Arabidopsis thaliana*, *Xanthomonas campestris pv. campestris* (*Xcc*), and the virulent phage Seregon. Parallel transcriptomic profiling shows that application of a single-phage treatment does not eradicate *Xcc* but strongly mitigates disease symptoms, restoring plant growth within 14 days post-inoculation. Phage-mediated protection is further associated with reduced plant immune activation, including lower jasmonate-related responses and reactive oxygen species levels, confirmed using nuclear reporter lines and histochemical staining. In parallel, *Xcc* shows reduced expression of key virulence-associated genes, including type III secretion system components, effectors, and flagella biosynthesis genes. Notably, phage treatment does not promote substantial resistance emergence in planta, contrasting with *in vitro* conditions. Together, our findings show that phage biocontrol can enhance plant resilience by modulating both host immunity and pathogen behavior.

INTRODUCTION

The escalation of bacterial plant pathogens,[1] coupled with the diminishing effectiveness of traditional antibacterial treatments due to overuse and shifting climatic conditions, threatens our food supply.[2,3] The increasing prevalence of antibiotic-resistant pathogens adds to the concern. In this context, microbe-based strategies present sustainable and effective alternatives to antibiotics, chemical fertilizers, and pesticides, which can have considerable impacts on human health and environmental sustainability.

Bacteriophages (phages) are specialized viruses that infect and eliminate bacteria. Their therapeutic potential in treating human or plant diseases was recognized early after their discovery more than a century ago.[4] However, interest declined with the rise of highly effective chemical biocides that offered broad-spectrum applicability. In the light of the growing antibiotic resistance crisis and the impacts of climate change, phage-based solutions are now regaining significant attention for their precision, effectiveness against plant pathogens, and safety for agricultural applications.[5,6] The advancement of these environmentally sustainable alternatives is reinforced by policies like the European Union's Green Deal, which targets a 50% reduction in synthetic agrochemical use by 2030 (https://food.ec.europa.eu/plants/pesticides/sustainable-use-pesticides_en). Versatile applicability of phages is shown by recent studies reporting on the development of effective phage-based sprays, soil treatment formulation and seed coatings.[7] Efficient phage-based biocontrol was demonstrated for some of the major plant pathogens, including *Pseudomonas syringae, Xanthomonas campestris*, *Xanthomonas oryzae*, *Erwinia amylovora*, *Ralstonia solanacearum*, *Pectobacterium carotovorum*, and *Xylella fastidiosa*, at several stages from *in planta* studies, green house trials, and in some rarer cases, in field studies as reviewed recently.[6,8]

Constantly exposed to various pathogens of bacterial, fungal, or viral origin, plants have developed intricate sensing and regulatory networks to fine-tune their immune response. The classic ZIG-ZAG model of plant immunity describes a multi-layered defense system featuring sequential activation to protect the plant.[9] If one layer fails, the activation of a subsequent layer can still provide resistance or, if ineffective, lead to susceptibility. The first layer of defense detects microbe-associated molecular patterns (MAMPs) via pattern recognition receptors (PRR), which recognize conserved bacterial features such as cell-wall

components[10–12] or flagellin.[13–16] One prominent example is the detection of the Flg22 region, though some *Xanthomonas* strains evade this recognition by modifying Flg22.[17] Detection by PRRs gets transduced by a cascade of mitogen-activated kinases (MAP-kinases) in the second layer of defense,[18–20] finally leading to transcriptional activation of defense genes and the so-called microbial pattern-triggered tmmunity (PTI). Pathogenic bacteria, including *X. campestris* (*Xcc*), deploy type 3 secretion systems (T3SS) to deliver effector proteins into the plant cell[21–25] to interfere with the PTI signaling cascade.[26] This defense layer is tuned to detect these effectors, either directly or indirectly,[27,28] and to activate heavy defense responses, e.g., production of reactive oxygen species or induction of cell death to prevent further spreading of the disease. If successful, this leads to effector-triggered immunity (ETI).[29] ETI also plays a crucial role in the interaction between *Xcc* and *Arabidopsis*.[30]

Local immune activation translates into systemic responses through defense-related plant hormones, including salicylic acid (SA),[31] jasmonic acid (JA),[32,33] ethylene (ET),[34] and abscisic acid (ABA).[35] These hormones induce systemic acquired resistance (SAR) by activating defense genes beyond the infection site.[36] However, defense responses are energy intensive, creating a trade-off with growth. Plants have one last trick up their sleeve: close monitoring of their environment and detection of bacterial signaling molecules like e.g., N-acetyl-homoserine lactones involved in bacterial quorum sensing, leading to low-level defense activation across the whole plant, enabling a rapid response upon pathogen attack.[37]

In this study, we focused on the biocontrol of *X. campestris* (*Xcc*), a major plant pathogen responsible for black rot disease in *Brassicaceae* like cabbage, broccoli, or rapeseed.[38,39] *Xcc* is a seed-transmitted bacterium with both epiphytic and endophytic vascular life phases.[40,41] Under favorable conditions and at high population densities, it enters the plant through natural openings, such as hydathodes, stomates, cracks, or wounds.[42,43] This collective invasion is coordinated by diffusible molecules and recognition systems, involving chemoattraction and quorum sensing systems.[44] Once inside the plant, *Xcc* establishes biofilms in the xylem, drawing nutrients from the sap. By clogging vascular bundles with biofilms and short-circuiting plant defense responses with effector proteins, *Xcc* causes the typical V-shaped necrotic lesions in important crop plants like *Brassica oleracea.*

While numerous historical and recent studies highlight the potential of phage-based biocontrol, comparatively little is known about how phage treatment of the pathogen influences plant immune responses and bacterial adaptation to phage predation within tripartite plant-pathogen-phage interactions. In this study, we established an *Arabidopsis thaliana-Xcc* system to assess the impact of phage biocontrol under controlled conditions. A single application of the virulent phage Seregon[45] mitigated disease symptoms and promoted recovery of plant growth within two weeks post-infection. Parallel transcriptomic profiling across infection stages revealed that the strong immune response triggered by *Xcc* in the host was attenuated when *Xcc* was applied together with the phage 2 and 7 days post-inoculation (dpi). Although bacterial populations were not fully eliminated, expression of key virulence- and motility-associated genes in *Xcc* was substantially reduced. Moreover, we detected no evidence for the rapid emergence of resistance against phage Seregon under these conditions. Together, these findings provide molecular support for how phage treatment modulates both host and pathogen responses within this tripartite interaction.

RESULTS

Phage biocontrol restores plant growth in the presence of the bacterial pathogen *Xanthomonas campestris*

To investigate phage-based biocontrol in a defined laboratory setting, we established a tripartite system consisting of the model plant *Arabidopsis thaliana*, the bacterial plant pathogenic organism *Xcc* and phage Seregon infecting *Xcc*.[4] For infection experiments we used a sterile plate-based system (Figure 1 A; B). While infection of *A. thaliana* with *Xcc* resulted in a significant reduction in leaf area and plant fresh weight, treatment with the phage strongly reduced the adversary effect of *Xcc* on *A. thaliana.* First phenotypic differences were noticed after 5 dpi. At 12 dpi, a significant difference in the leaf area and plant fresh weight was observed between the control and the *Xcc* treatment (Figures 1C and 1D). Throughout the experiment (0–14 dpi), there was no significant difference between the leaf area of the control, the phage-only condition and the phage biocontrol treatment against *Xcc* at a multiplicity of infection (MOI) of 5 (*Xcc* + Φ = five phages per bacterial cell).

To quantify the effect of phage biocontrol on the abundance of bacterial cells and infectious phage particles, we determined bacterial cfu mg-1 plant fresh weight as well as phage Seregon pfu mg-1 (Figure 1E). We observed a 10-fold reduction of bacteria over the course of the experiment. Phage titers declined over the course of the experiment but stayed consistently higher in the biocontrol condition (presence of *Xcc* as host) in comparison to the phage-only control. While the bacteria were not eradicated by this single phage treatment, plant growth was nevertheless restored to the level of the uninfected control underlining the efficacy of phage pressure in this setting and its potential for biocontrol applications.

Tripartite transcriptomic analysis of phage-based biocontrol

To gain insights into plant defense signaling and bacterial response to phage treatment, we performed a comprehensive tripartite parallel transcriptomic study. All samples were processed via a double rRNA depletion for plants and prokaryotes, prior to sequencing. Across all conditions, we detected 76% of all *Arabidopsis* genes, 73% of *Xcc* genes, and 92% of phage Seregon genes. Only in one sample, at 7 dpi, no phage reads were detected.

Principalcomponent analysis (PCA) plots of plant samples show clear separation of treatment and time-point dependent changes (Figure 2A). To understand how *Arabidopsis* responds to *Xcc* in the presence or absence of phage Seregon, we performed an analysis of differential expressed genes (DEGs) of each treatment compared to untreated plants at the same developmental time point. In line with the phenotypic data (Figure 1B), pathway enrichment analysis using the Kyoto Encyclopedia of Genes and Genomes (KEGG) database revealed 17

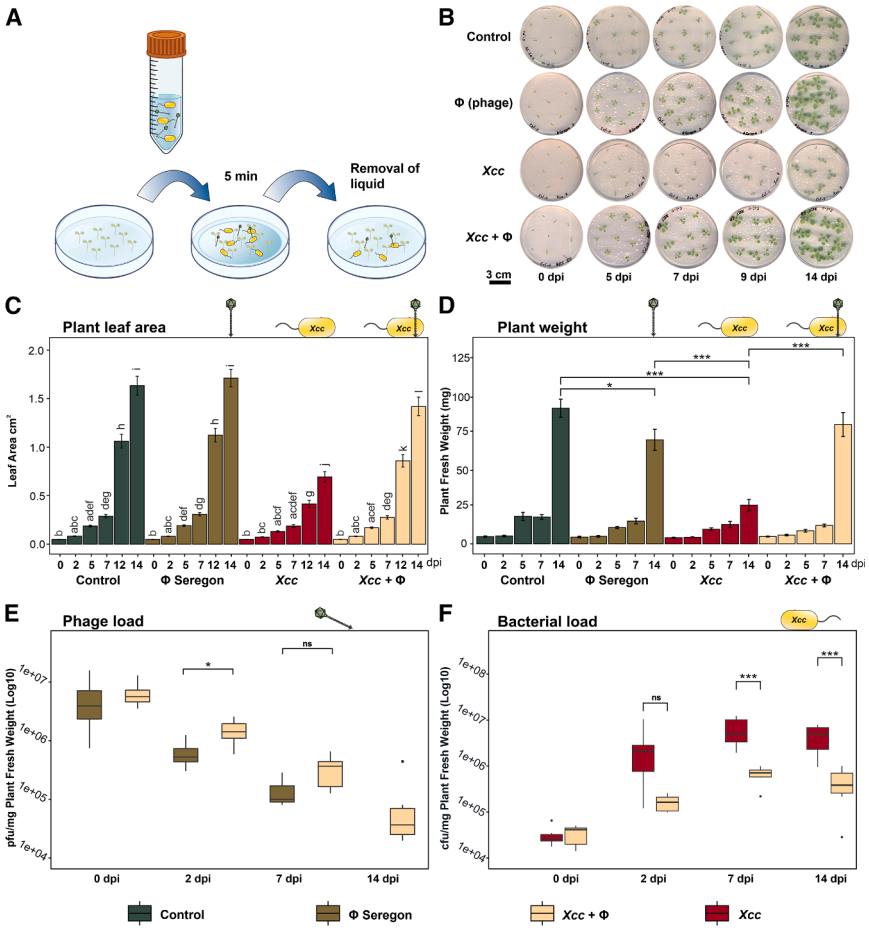

Figure 1. Phage mediated plant protection over time—tripartite interaction in a tripartite system and plant phenotyping

(A) Inoculation workflow.

(B) Depiction of the plants over time showing the control-inoculated plants (first row, ½ MS media only), *X. campestris* (second row), *Xcc* plus phage at *Xcc* + ϕ (third row), phage Seregon (forth row).

(C) Non-invasive measurement of leaf area over time. ANOVA test followed by Tukey HSD F(3.234) = 31.25, $p = 0.0001$, shown as compact letter display (CLD). (n = 200 plants per condition for 0 dpi, n = 166 plants per condition for 2 dpi, n = 129 plants per condition for 5 dpi, n = 84 plants per condition for 7 dpi, n = 61 plants per condition for 12 dpi, and n = 57 for 14 dpi).

(D) Fresh weight per plant over time. ANOVA test followed by Tukey HSD F = 48.38, $p = 8{,}62e{-}67$). (n = 12 plants per condition for 0 dpi, n = 12 plants per condition for 2 dpi, n = 6 plants per condition for 5 dpi, n = 9 plants per condition for 7 dpi, n = 20 plants per condition for 14 dpi). Asterisks indicate significance for the 14 dpi time point; (*) $p < 0.05$; (**) $p < 0.01$, (***) $p < 0.001$.

(E) Phage load per mg of plant fresh weight.

(F) Bacterial load per mg of plant fresh weight. Asterisks (*) in (E) and (F) indicate significance after a pairwise comparison using Student's *t* test, (n = 6 plants for 0, 2, 7 dpi and n = 10 for 14 dpi); for each time point (*) $p < 0.05$; (**) $p < 0.01$, (***) $p < 0.001$. Error bars in (C) and (D) represent standard error of the mean (SE), in (E) and (F) we show standard boxplots, with whiskers extending to 1.5 × interquartile range (IQR).

immune-related pathways upregulated in *Xcc*-treated plants at 2 dpi (Figure 2C upper). In contrast, phage-treated samples only revealed 3 upregulated pathways. By 7 dpi, seven pathways remained enriched, with a role in secondary metabolite production. To further visualize the plant response under phage biocontrol conditions, we compared DEGs and looked for enriched pathways during biocontrol. Pathway enrichment showed that 3 distinct pathways are downregulated under biocontrol conditions compared to *Xcc*-infected plants at 2 dpi; carotene catabolic process, terpene catabolic process, and isoprenoid catabolic process, whereas at 7 dpi only one pathway, related to RNA modification, was upregulated (Figure 2C). The carotenoid pathway is linked to ABA biosynthesis and redox regulation.[47] Terpenes, which are plant secondary metabolites often induced by elicitors, exhibit antimicrobial activity,[48,49] similar to isoprenoids—particularly those derived from the mevalonate (MVA) pathway.[50] The observed downregulation of these 3 plant pathways under phage-biocontrol conditions suggests a suppressed immune response compared to plants infected with *Xcc*. Notably, some of the most strongly downregulated genes in phage-treated, infected plants include key regulators of programmed cell death (BAP2), ABA signaling (CML 37), redox regulation (AOX1D), and immunity regulation via JA (WRKY59) (Figure 2D).

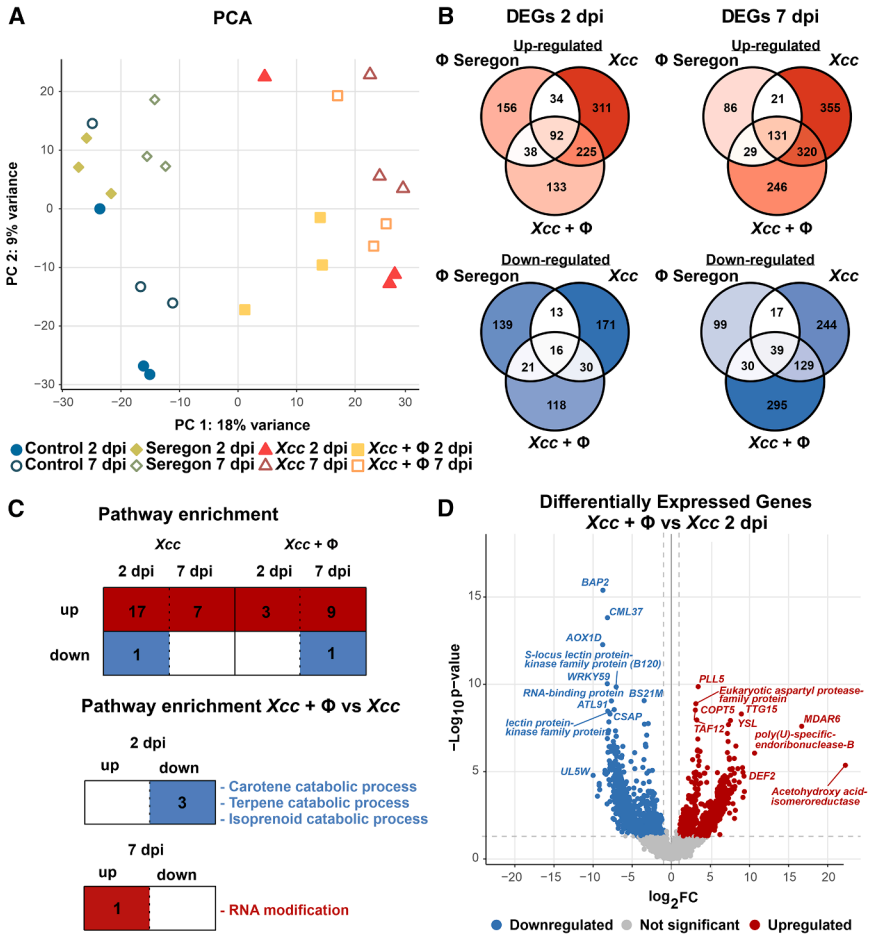

Figure 2. Differentially expressed Arabidopsis genes point toward a reduced need for full defense activation during tripartite interaction

Significant differentially expressed genes (DEGs) were identified using the DESeq2 algorithm.[46]

(A) Principal-component analysis of expressed plant genes. Samples are colored according to their treatment condition.

(B) Venn diagram of differentially expressed genes during tripartite interaction. Upregulated genes are displayed in red, downregulated genes are displayed in blue. Each condition was tested against the control at the respective development time point which was used as a reference (p value <0.05). The resulting condition-specific differentially expressed genes were then compared to every other condition to see if there is an overlap.

(C) Significantly enriched KEGG pathways (Table S1). Upper table: compared to day-specific control; lower table: biocontrol compared to *Xcc*-infected plants.

(D) Volcano plot of phage treatment (*Xcc*+ ϕ) compared to *Xcc* conditions, 2 dpi. Downregulated genes are displayed in blue, whereas upregulated genes are shown in red. Dotted gray lines indicate the significance threshold (p value <0.05 and Log2 foldchange >1). The ten most significant differentially expressed are displayed with gene names.

Infection with Xcc triggers significant plant defense signaling

Upon *Xcc* infection, *Arabidopsis* exhibited a strong immune response reflected on the level of transcription (Figures 2B and 2C). Both pattern-triggered immunity (PTI) and effector-triggered immunity (ETI) are strongly upregulated at 2 and 7 dpi, signaling active pathogen recognition and defense activation (Figure S1). Notably, a broad range of nucleotide-binding leucine-rich repeat (NLR) proteins are induced, with *TIR-NBS6* (AT1G72890) showing a Log2FC ~7.6 at 2 dpi, highlighting a robust ETI response.

During signal integration, key defense-related kinases are strongly upregulated. Several genes encoding MAP kinases, cysteine-rich receptor-like kinases (CRKs), and transcription factors (WRKY, NAC, and MYB) exhibited increased expression levels. *CRK13* and *CRK24*, implicated in cell death and defense signaling, showed strong induction at both time points. In particular, *CRK13*, which is linked to cell death initiation, was upregulated across multiple variants. Additionally, calcium signaling components, including *CAR1* (AT5G37740) and calmodulin *CAM8*, are significantly induced, supporting their role in amplifying the immune response.

Defense execution mechanisms are also activated, including genes involved in reactive oxygen species (ROS) production and lignification. Peroxidases such as *PRX2*, *IRR1*, and *PER28* exhibited increased expression, indicating elevated oxidative stress and cell wall fortification against *Xcc*. These findings underscore the extensive immune activation triggered by *Xcc*, characterized by strong PTI and ETI induction, ROS production, and transcriptional reprogramming toward defense.

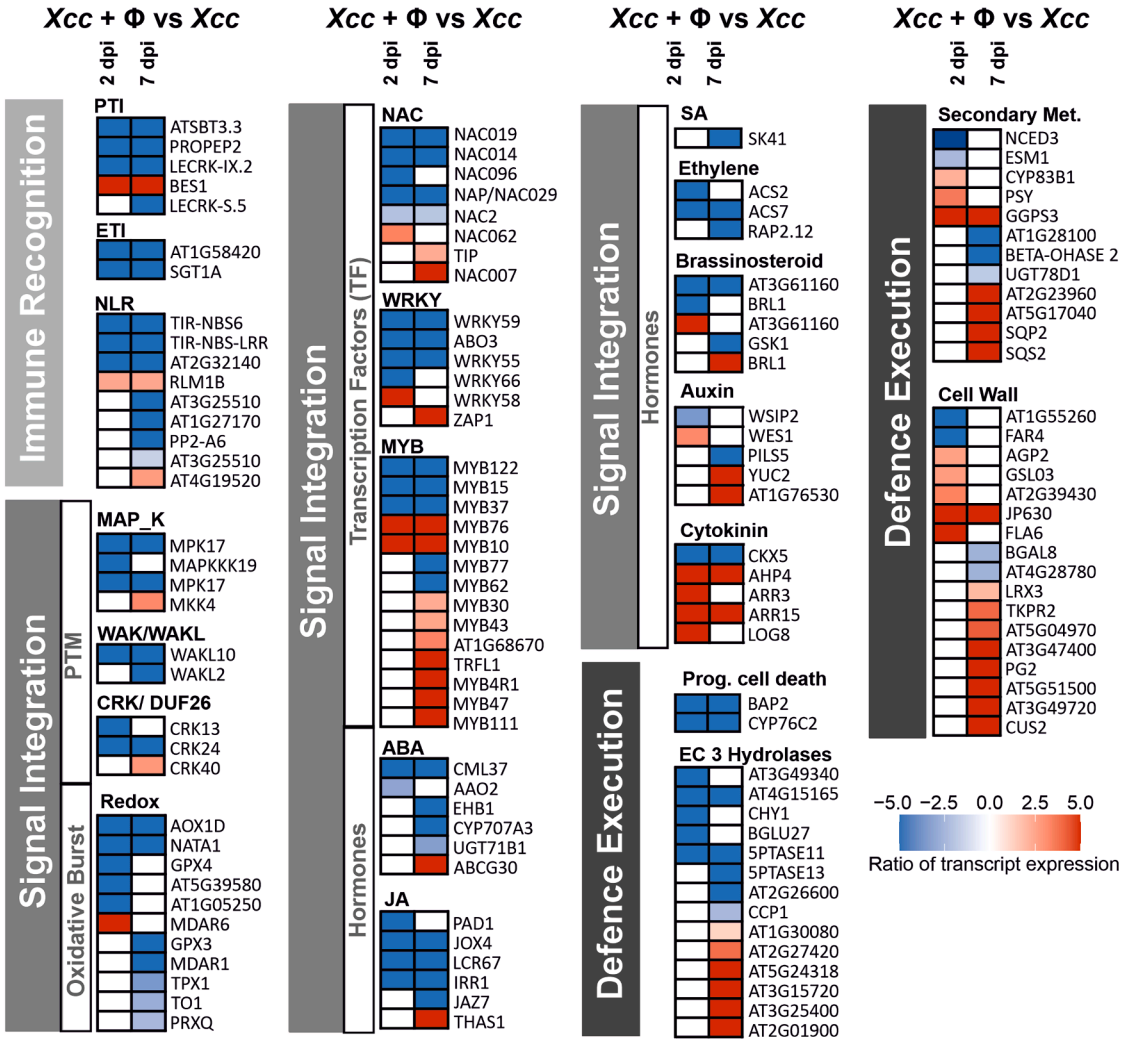

Figure 3. Phage biocontrol leads to altered defense regulation in Arabidopsis compared to the pathogen

Ratio of transcript expression of *Xcc* + ϕ compared to Xcc-infected plants (expressed as log2 (FC)). Shown are selected transcripts involved in pathogen recognition (light gray vertical bars) immune signal integration (medium gray) and defense execution (dark gray). The level of transcript expression is presented as a heatmap, shown bottom right, with shades of blue indicating lower expression, and shares of red indicating higher expression. The heatmap is cut off at ±5 for visual simplification, numerical data can be found in Table S2. Transcripts are grouped in functional groups based on MapMan mapping file X4.1,[52] with adaptations as listed in Table 2. Ratio of transcript expression compared to the mock-treated plants are shown in Figure S1 as well as a heatmap of the most significantly altered targets in *Xcc* + ϕ compared to Xcc-infected plants shown in Figure S2. Where discussed in the text protein kinases, transcription factors, redox, and hormone transcripts are linked through the use of symbols listed in the legend.

Phage-based biocontrol is associated with reduction in plant immune activation

To gain deeper insights, which genes are particularly responsive under conditions of phage biocontrol (*Xcc* + ϕ), we compared the transcript levels of *Xcc* + ϕ-treated to *Xcc*-infected plants. Accounting for the *p* value and the level of fold change, the 100 most significantly regulated genes are presented in Figure S2. The identified genes primarily fall into the following categories: PTI, ETI, oxidative burst, transcriptional activators, hormonal signaling, and cell death. The most striking regulation was seen in the expression of genes encoding a cutin synthetase (CUS2, AT5G33370), upregulated at 7 dpi, a loricrin-like protein (AT5G09670) as well as MDAR6 (AT1G63940) involved in redox regulation upregulated at 2 dpi. Strongest downregulation was found in a cytosolic invertase (CINV1, At1g35580), involved in sucrose conversion to fructose and glucose.

A selection of transcripts, with functional annotations matching the three stages of plant immunity (immune recognition, signal transduction, and defense execution pathways), as outlined in Wang et al.,[51] is summarized in Figure 3 (numerical values in Table 2). Among genes related to immune recognition, encompassing PTI, NLRs, and ETI, we observed downregulation of PTI transcripts ATSBT3.3, PROPEP2—a MAMP receptor, LECRTK-IX.2 at both days, and of LECRTK-IX.2 at 7 dpi. Interestingly BES1, which links bacterial response to the brassinosteroid

signaling pathway[53] is upregulated 7-fold in *Xcc* + ϕ at both time points. PROPEP2 regulation was confirmed in additional experimental round via quantitative reverse-transcription PCR (RT-qPCR) shown in Figure S3. In the group of NLRs, intracellular receptors that detect xenobiotic compounds within the cytosol, a number of Toll-interleukin-resistance (TIR) domain family proteins are downregulated in *Xcc* + ϕ plants. In the group of ETI transcripts, the genes SGT1A and At1g58420 are both downregulated in phage-treated plants at both time points.

Signal transduction involves protein kinases (MAPKs, WAK/WAKL, and CRK/DUF26), redox regulators, transcription factors (WRKY, NAC, and MYB), and hormone signaling. Among the genes encoding transcription factors, we observed lower transcript levels for WRKY and NAC transcription factors (e.g., WRKY59, WRKY55, NAC019, and NAC029) but increased expression of WRKY58, ZAP1, NAC062, and NAC007. NAC062 is relevant because it relocates to the nucleus under endoplasmatic reticulum stress and integrates biotic and abiotic stress responses, promoting cell survival[54] (Figure 3).

Notably, the group of MYB transcription factors deviates from the pattern of general downregulation during biocontrol. Here, we see a constitutive downregulation of MYB 15, MYB37, and MYB 122. However, a much larger group of seven MYB transcription factors is upregulated at 7 dpi (Figure 3). Among them, MYB111 encodes a master regulator of flavonoid synthesis[55] and could indicate shifts in secondary metabolism.

In the signal transduction subgroup related to hormonal signal integration, we selectively show the ABA, ethylene, and JA transcripts (full dataset- Table S6). The ABA signaling regulator CML37, a positive modulator of stress responses,[56–58] is downregulated at both time points. Decreased ABA synthesis is indicated already at 2 dpi with a downregulated abscisic aldehyde oxidase (AAO2). Transcripts involved in ABA conjugation and degradation (abscisic acid UDP-glycosyltransferase UGT71B1, abscisic acid hydroxylase CYP707A3), as well as ABA perception and signaling (EHB1), are all downregulated at 7 dpi. In contrast, ABA transporter ABCG30 is upregulated at 7 dpi (Figure 3).

Among genes involved in auxin transport, *PILS5*, a growth inhibitor under stress conditions,[59] is suppressed, while *PIN-LIKES4* is upregulated, potentially promoting normal growth (Table 2). Ethylene signaling is downregulated constitutively in *Xcc* + ϕ plants, with the ethylene synthesis related transcripts ACS2 and ACS 7 downregulated at 2 dpi and both time points, respectively. In addition, RAP2.12 involved in ethylene signaling is downregulated at 7 dpi.

Similarly, the jasmonate pathway showed a general downregulation. At 2 dpi, *PAD1*, required for jasmonate signaling,[60] is downregulated in phage biocontrol compared to *Xcc*-infected plants, along with IRR1, *JAZ7*, *Pdf1.1*, and *JOX4*— jasmonate induced oxygenase 4 (Figure 3). This is in line with the previously described downregulation of the jasmonate-responsive transcription factor *WRKY59*. We further confirmed this via RT-qPCR where we showed downregulation of *WRKY59* and further targets at 2 dpi in an independently conducted experiment (Figure S3).

The final set of transcripts examined here belongs to the defense execution step. Markers of hypersensitive response (HR) and cell death are notably downregulated, supporting our expectation that biocontrol limits excessive immune activation. *CYP76C2*, a cytochrome P450 involved in HR, is strongly suppressed (Log2FC -8.1). Similarly, *BAP2*, a key regulator of programmed cell death required for the IRE1-mediated UPR is downregulated at 2 dpi (Log2FC -8.7 and -8.3*).

At the structural level, cuticle biosynthesis is reinforced through upregulation of *CUS2*[61] and a loricrin-like peptide,[62] with lipid metabolism genes (*MBOAT*, *LPXA*, *ELT6*, and *ALT1*) supporting suberization. RNA signaling is affected via *MORF1* upregulation, while the strong downregulation of *CINV1* suggests limited pathogen access to plant energy resources.[63] Additionally, programmed cell death regulators *CYP76C2* and *BAP2* are significantly suppressed.

Overall, these findings indicate that phage biocontrol is associated with reduced immune activation by lowering pathogen burden and preventing excessive defense-associated stress, allowing the plant to maintain growth and metabolic balance.

Nuclear localized reporter plant lines confirm reduced ROS and jasmonate response in phage-biocontrol plants

One major driver of defense-associated stress is damage caused by free radicals during the generation of ROS. Transcriptomic data suggested reduced ROS production under biocontrol conditions, with ROS inhibiting genes being downregulated after 2 dpi. For instance, the alternative oxidase 1D (AOX1D), which minimizes oxidative stress,[64] is strongly downregulated (logFC −8.7), as is NATA1, a negative regulator of hydrogen peroxide. Additionally, cysteine-rich RLK (RECEPTOR-like protein kinase) 24 is significantly downregulated (log2FC −6.3).

To test the hypothesis that immune responses triggering ROS production are differentially regulated in presence or absence of phages, we used PER5:3xVenus-NLS lines of *Arabidopsis*.[65] Here, the nuclear localized Venus reporter gene is fused to the PER5 promoter. PER5 encodes the microsomal ASCORBATE PEROXIDASE 5 involved in scavenging of hydrogen peroxide, resulting in increasing fluorescence signal in the nucleus under oxidative stress (Figures 4 A and 4B). In our tripartite setting, *Xcc*-treated plants showed strong nuclear fluorescence accumulation in roots, while *Xcc* + ϕ-treated plants exhibited a much weaker signal, consistent with lower ROS levels and corroborating the hypothesis of a reduced immune response under phage biocontrol conditions. We further confirmed this observation by histochemical staining of hydrogen peroxide (H_2O_2) levels in plant tissue in an independent experimental round for the wild type Col-0 as well as the PER5:3xVenus-NLS lines of *Arabidopsis* (Figures S4 and S5).

In similar manner, we tested if phage biocontrol (Xcc + ϕ) will result in decreased expression of jasmonic acid synthesis gene as observed in the transcriptomics results, utilizing the AOS (At5g42650) promotor coding for a triple venus with a nuclear localization tag.[66] Here, the promoter of the gene encoding the JA synthesis protein AOS was coupled to the Venus reporter gene. Consistent with transcriptomic data, *Xcc*-treated roots showed strong JA-related signal accumulation, whereas under phage biocontrol conditions, plants had significantly lower levels.

Phage biocontrol leads to reduced expression of bacterial virulence genes

To better understand how phage biocontrol influences *Xcc* during plant infection, we analyzed bacterial gene expression in the

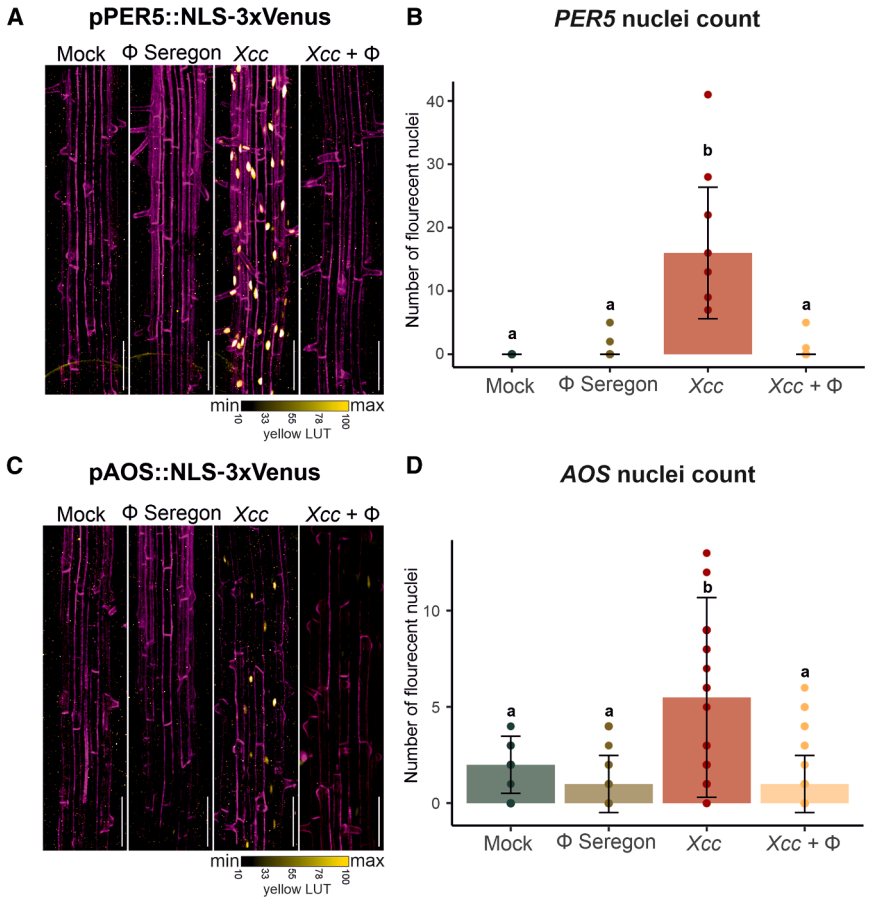

Figure 4. Nuclear localized reporter plant lines confirm reduced ROS and jasmonate response in phage-biocontrol conditions

(A) Peroxidase superfamily reporter PER5[66] induction (yellow) co-visualized with propidium iodide stained cell walls (PI, magenta), in response to *Xcc*, phage Seregon, and *Xcc* + ϕ.

(B) Nuclei count in PER5 reporter lines; Different letters indicates significance after Kruskal-Wallis test, chi-squared = 20.387, df = 3, *p* value = 0.0001411.

(C) Jasmonic acid synthesis reporter line AOS (yellow) co-visualized with propidium iodide-stained cell walls (PI, magenta response to *Xcc*, phage Seregon, and *Xcc* + ϕ. Microscopic images are presented as maximum Z projection.

(D) Nuclei count in AOS reporter lines; quantification of bright nuclei is given as a bar plot with median ± mad (median absolute deviation), significant differences -indicated with different letters were calculated with Kruskal-Wallis test, chi-squared = 15.091, df = 3, *p* value = 0.001741, (n = 7). Individual measurements are presented as data points. Scale bars, 100 μm. See Figures S4 and S5 for further information via histochemical staining.

presence and absence of phage Seregon. PCA analysis revealed distinct bacterial transcriptomic profiles, with the strongest differences occurring at 2 dpi (Figure 5A; Figure S3D). Differential expression analysis showed a significant shift in bacterial gene regulation under phage pressure (Figure 5B), with a marked reduction in virulence-associated genes and an increase in stress response pathways.

Remarkably, phage infection led to the downregulation of multiple *Xcc* virulence factors, particularly key T3SS components and effectors (*hrpF*, *xopX*, *xopE*, and *xopAH*), likely hampering effector protein delivery required for plant colonization (Figures 6A and 6B; Figure S3B).[67] Additionally, genes encoding enzymes involved in plant cell wall degradation (M91 metallopeptidase, pectate lyase, and cellulase) showed reduced expression levels, along with *gspD*, a component of the T2SS secretion system, further limiting bacterial invasion. Reduced motility was indicated by the strong downregulation of *fliA*, the flagellar biosynthesis sigma factor, which may restrict systemic spread within *Arabidopsis* and is also associated with bacterial virulence. Interestingly, *Xcc* antioxidant defenses were also affected, with catalase genes *katB* and *katG* being significantly downregulated.[68] This may result from lower overall ROS levels in phage-biocontrol plants. Another notable finding was the suppression of *qatB* and *qatC*, encoding components of the QatABCD anti-phage defense system. The observation that amongst the bacterial transcripts during biocontrol anti-phage systems were downregulated is counterintuitive at first glance but might hint toward a phage-mediated suppression of bacterial defense.[69]

Coexistence of phage Seregon and *Xcc* did not lead to enhanced emergence of bacterial resistance to phage infection

In our transcriptome analysis, we detected phage Seregon transcripts in infected plants (Figure 6C) at all time points. These

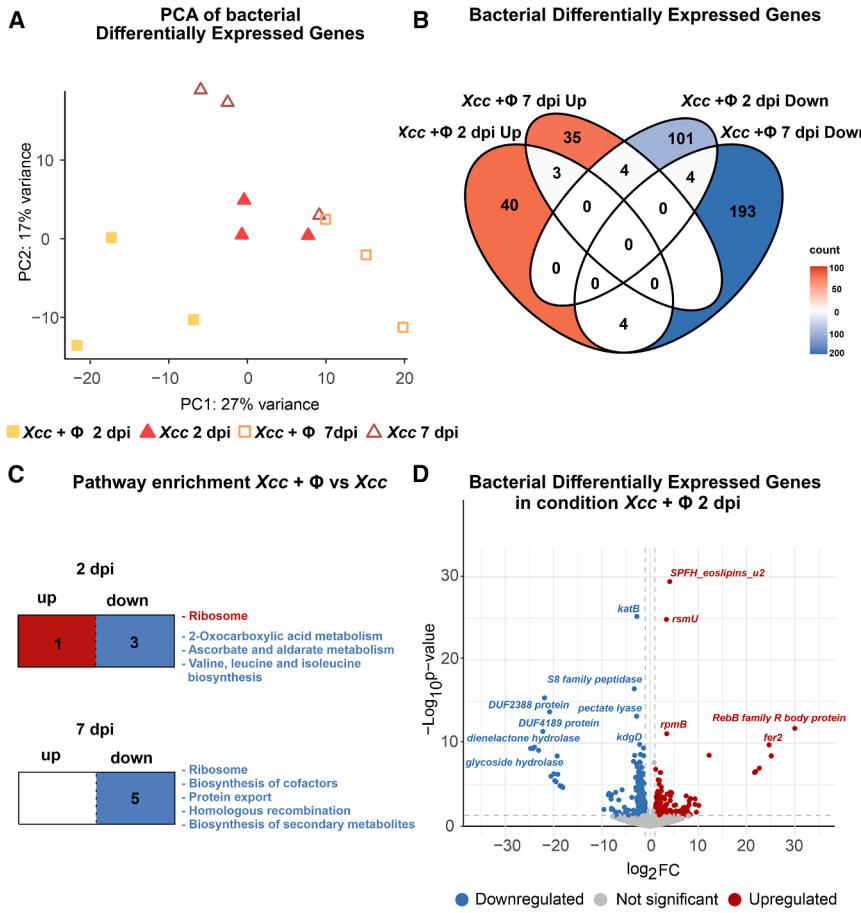

Figure 5. Phage biocontrol results in reduced expression of bacterial virulence-associated genes

Differentially expressed bacterial genes were identified with DESeq2; *p* value <0.05.

(A) Principal-component analysis, samples: bacterial reads from samples *Xcc* + ϕ 2 dpi, *Xcc* + ϕ 7 dpi, *Xcc* 2 dpi, and *Xcc* 7 dpi.

(B) Venn diagram of differential expressed genes in the presence of phages (*Xcc* + ϕ) and the *Xcc* (Figures S3 and S4).

(C) Number of enriched pathways (Table S4).

(D) Volcano-plot of differentially expressed genes. Upregulated genes are marked in red, downregulated genes are marked in blue.

results confirmed that phage biocontrol—as applied in our study—did not lead to the eradication of the pathogen *Xcc*, thereby enabling ongoing infection of *Xcc* by Seregon. Nevertheless, Seregon pfu's significantly declined over the course of the experiment (Figure 1E). Therefore, we wondered whether phage-treatment might lead to the emergence of bacterial resistance to phage infection. To test this, we isolated *Xcc* cells through an invasive harvest (Figure 1F) and submitted surviving clones of *Xcc* to a phage sensitivity testing. Remarkably, only 6-10% of the surviving colonies retrieved from the plants were resistant to phage Seregon (Figures 6D and S7). In contrast, 97% of colonies isolated from an *in vitro* infection experiment were resistant. These results highlight the promising potential of phage-based biocontrol in reducing bacterial virulence while not leading to quick emergence of phage resistance in complex and structured environments like in the plant context. To identify the potential phage receptor, we sequenced four resistant *Xcc* clones resulting in 23 unique SNPs (Table S4). Mutations in a gene encoding a glycosyl transferase (XC_4244) and conserved hypothetical membrane protein DUF885 (XC_1704) provide first hints that glycosylation of cell wall components might be relevant for host recognition. Indeed, a knock-out of XC_4244 conferred partial resistance against phage Seregon (Figure S8).

DISCUSSION

Bacteriophages remain an underutilized resource that bears a high potential for the development of sustainable biocontrol strategies against plant pathogenic bacteria. This potential arises from key characteristics of lytic phages: their host specificity and ability to self-propagate. In this study, we demonstrated that treatment with the virulent phage Seregon sufficiently inhibited the *Xcc* infection and in turn, effectively protected *A. thaliana* seedlings, restoring leaf area and plant weight to control levels. Our tripartite-transcriptomic analysis revealed that phage biocontrol was associated with reduced plant defense investment in the presence of the pathogen under phage predation. While a single phage treatment did not completely eradicate

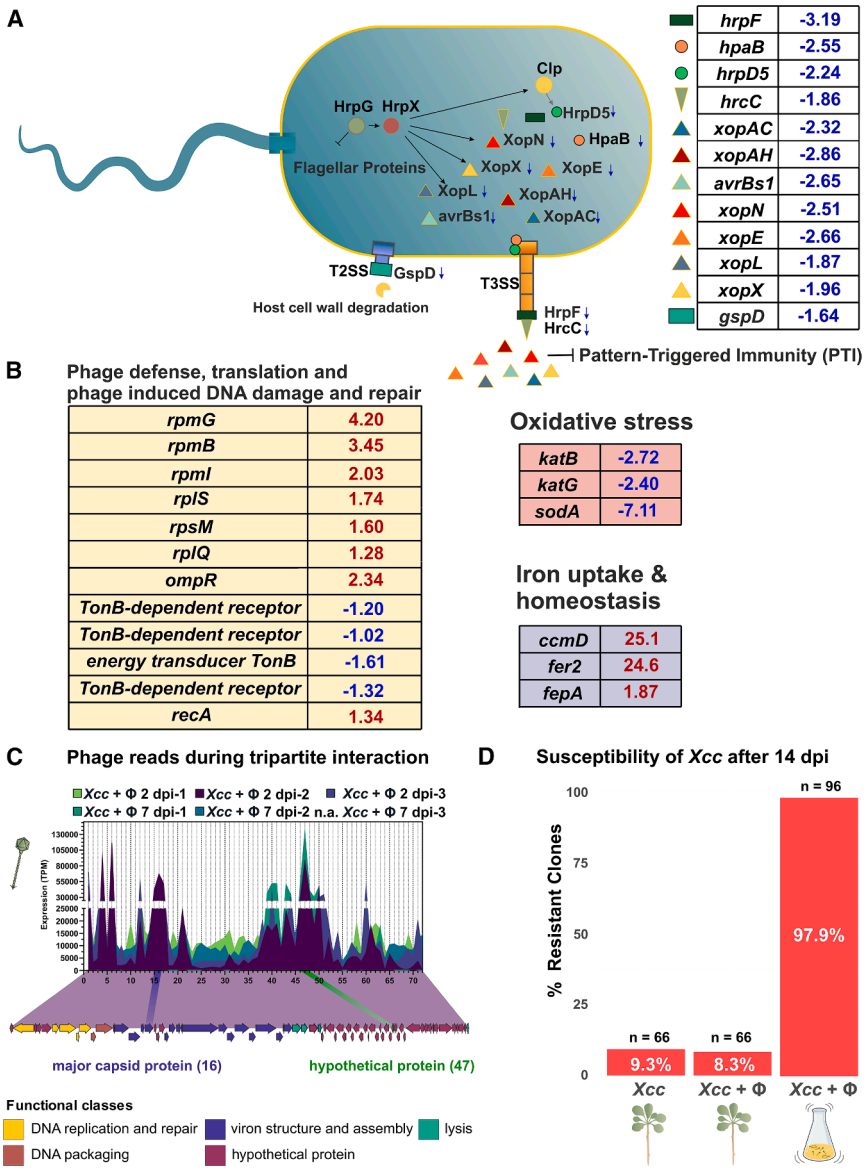

Figure 6. Bacterial virulence expression and phage transcripts

(A) Significant differentially expressed effector genes (log2fold change) involved in *Xcc* virulence are presented in their regulatory context. Selected targets were further confirmed by qPCR (Figure S3).

(B) Further functional bacterial clusters under *Xcc* versus *Xcc* + ϕ (log2fold change).

(C) Transcripts mapping to the genome of phage Seregon.

(D) Susceptibility testing to phage Seregon of *Xcc* colonies (n = 66) surviving after 14 days *in planta* in presence and absence of phage compared to 14 days incubation in a batch *in vitro* culture.

Xcc, it significantly suppressed the expression of virulence genes in *Xanthomonas*, highlighting its potential as a biocontrol strategy.

Our study provides insights into the impact of phage biocontrol on plant immune signaling and bacterial adaptation at the level of gene expression. We found that phage biocontrol is associated with a reduced expression of bacterial virulence-associated genes, allowing the plant's PTI to effectively counter the pathogen. We observed alterations in ETI, hormonal signaling, and cell death regulation under phage biocontrol, which is in line with improved plant survival and performance under pathogen pressure. In agreement with these findings, phage-biocontrol plants upregulate cytokinin biosynthesis (LOG8) and perception transcripts (AHP4, ARR3, and ARR15) indicating a shift toward enhanced growth and development.[70,71]

Past studies already revealed the strong potential of bacteriophages in controlling crucifers' black rot, from early proposals a century ago[4] to recent systematic testing of *Xanthomonas*

phages in plant nurseries.[72,73] Significant symptom reduction, effective seed decontamination, and lower bacterial load in treated plants have been identified.[72] Consistent with our results, they also found that bacterial resistance emergence *in planta* remains limited.[74–76] Others observed reduced bacterial virulence in the phage resistant subpopulation of the pathogen.[77,78] This underscores the value of *in planta* studies, since *in vitro* assays—despite their high throughput—do not capture the physiochemical complexity of the plant environment that is essential for understanding phage-host interactions. To improve future approaches, the design of complementary phage cocktails or phage engineering can further enhance biocontrol efficacy and mitigate resistance development.[5]

The critical role of secretion systems for *Xanthomonas* virulence is well established.[67,79,80] In line with the restoration of plant growth, we observed significantly reduced expression of virulence-associated genes in phage-treated samples. Specifically, we detected downregulation of the T2SS outer membrane translocon GspD, which is important for transporting folded proteins into the periplasm.[81] In addition, genes encoding components of the T3SS translocon HrpF and several T3SS effectors showed reduced expression. Among these, the secreted effector XopN—previously shown to interfere with receptor-like kinase (RLK) function in tomato and thereby hampering PTI[82]—was notably reduced, further supporting the impact of phage biocontrol in weakening bacterial virulence at the plant environment.

While most studies have focused on the interactions between bacteria and phages or between bacteria and plants, the potential for a direct interaction between plants and phages remains unknown. In mammalian models, phages exhibit niche specialization and influence immune modulation.[83,84] Studies have shown that phages adhere to the human mucus, enabling their persistence within this niche.[84,85] Likely similar and highly complex niche adaptations occur for phages in the plant environment.[7] Interaction with "non-host" organisms, like fungal hyphae, was further shown to be involved in the transport of phages to new soil habitats.[86] First attempts also studied translocation of phages in the plant system but did not yet provide mechanistic insights.[87,88] Notably, the coexistence of bacteria and phages was not driven by a widespread development of phage resistance within the bacterial population in planta. This suggests that phage resistance entails fitness trade-offs for the pathogen in the host environment. This is in line with coevolution experiments by others.[75] It remains an intriguing question whether plants have evolved mechanisms that modulate phage activity, as recently proposed for bacterial communities.[89]

While our parallel transcriptomics approach represents an important first step, future research should further elucidate the molecular mechanisms underlying viral perception and immune homeostasis within both synthetic and native plant-microbe consortia. In particular, validation of the native host plant of *Xcc*, the economically important crop *Brassica oleracea*, will be essential to assess the robustness and transferability of our findings under agriculturally relevant conditions. Extending these insights to crop systems will facilitate the translation of fundamental knowledge into practical and sustainable disease management strategies. A deeper molecular understanding of these complex interactions is essential for the rational design of effective and sustainable phage-based biocontrol strategies.

Limitations of the study

While the study provides unprecedented depth of understanding of the tripartite interaction between plant, bacteria and phage, it is an *in vitro* study and, as such, the responses may vary compared to real life conditions e.g., in the field. Future efforts based on greenhouse experiments in soil are already developing in this direction. Furthermore, while we see a clear downregulation of plant immunity under phage biocontrol conditions, this coincided with both decreased bacterial numbers as well as reduced expression of bacterial virulence genes. Thus, the attenuated plant immune response may result from reduced pathogen load, altered physiology of surviving bacteria under phage pressure, or a combination of both. Future experiments using bacterial load assays *in planta*, single-cell reporters, or re-isolated bacterial populations grown under standardized conditions would help to distinguish direct phage-driven virulence modulation from population-size effects.

RESOURCE AVAILABILITY

Lead contact

Requests for further information and resources should be directed to and will be fulfilled by the lead contact, Borjana Arsova (b.arsova@fz-juelich.de).

Materials availability

All unique reagents generated in this study are available from the lead contact without restriction.

Data and code availability

- RNA-seq data have been deposited at Gene Expression Omnibus and are publicly available at GEO: GSE294853 *https://www.ncbi.nlm.nih.gov/geo/query/acc.cgi?acc=GSE294853*
- Code: this study does not report original code.
- Any additional information required to reanalyze the data reported in this paper is available from the lead contact upon request.

ACKNOWLEDGMENTS

The authors gratefully thank Prof. Dr. Franz Narberhaus (RUB, Bochum) for providing the *Xanthomonas campestris* 8004 strain, Michaela Gerads for technical assistance and all teams for the supportive working environment. We thank the German Research Foundation (CRC 1535 "Microbial Networking", project ID 45809066; DFG Heisenberg Professorship, GR4559/4-1; and CEPLAS-EXC-2048/1-project ID 390686111) for funding.

AUTHOR CONTRIBUTIONS

S.H.E., B.A., U.S., and J.F. designed the study. S.H.E., M.T.K., S.S., and M.Z. performed the experiments. S.H.E. and B.A. performed the RNA-seq data analysis. M.Z. performed microscopy and image analysis. S.H.E., G.G., J.F., and B.A. wrote the manuscript. B.A., U.S., G.G., and J.F. supervised the experiments. All authors read, revised, and approved the final manuscript.

DECLARATION OF INTERESTS

The authors declare no competing interests.

STAR★METHODS

Detailed methods are provided in the online version of this paper and include the following:

- KEY RESOURCES TABLE
- EXPERIMENTAL MODEL
  - Plant propagation
  - Bacterial growth conditions
  - Phage amplification
- METHOD DETAILS
  - Plant inoculation
  - Non-invasive plant phenotyping
  - Invasive plant phenotyping and extraction of microbes
  - RNA extraction
  - RNA-seq
  - Imaging of nuclear reporter lines
  - Histochemical staining of reactive oxygen species
  - RT-qPCR
- QUANTIFICATION AND STATISTICAL ANALYSIS
  - Quantification of green area during non-invasive plant phenotyping
  - Differential expression analysis of RNA-Seq
  - Quantification of images of nuclear reporter lines
  - Quantification of histochemical staining of reactive oxygen species
  - Statistical analysis of qRT-PCR results of plant and bacterial transcripts

SUPPLEMENTAL INFORMATION

Supplemental information can be found online at https://doi.org/10.1016/j.celrep.2026.117622.

Received: May 23, 2025
Revised: March 2, 2026
Accepted: June 10, 2026
Published: June 30, 2026

REFERENCES

1. Mansfield, J., Genin, S., Magori, S., Citovsky, V., Sriariyanum, M., Ronald, P., Dow, M., Verdier, V., Beer, S.V., Machado, M.A., et al. (2012). Top 10 plant pathogenic bacteria in molecular plant pathology: Top 10 plant pathogenic bacteria. Mol. Plant Pathol. *13*, 614–629. https://doi.org/10.1111/j.1364-3703.2012.00804.x.
2. McManus, P.S., Stockwell, V.O., Sundin, G.W., and Jones, A.L. (2002). Antibiotic use in plant agriculture. Annu. Rev. Phytopathol. *40*, 443–465. https://doi.org/10.1146/annurev.phyto.40.120301.093927.
3. Miller, S.A., Ferreira, J.P., and LeJeune, J.T. (2022). Antimicrobial Use and Resistance in Plant Agriculture: A One Health Perspective. Agriculture *12*, 289. https://doi.org/10.3390/agriculture12020289.
4. Mallmann, W.L., and Hemstreet, C. (1924). Isolation of an inhibitory substance from plants. J. Agric. Res. *28*, 599–602.
5. Czajkowski, R., Roca, A., and Matilla, M.A. (2025). Harnessing Bacteriophages for Sustainable Crop Protection in the Face of Climate Change. Microb. Biotechnol. *18*, e70108. https://doi.org/10.1111/1751-7915.70108.
6. Holtappels, D., Fortuna, K., Lavigne, R., and Wagemans, J. (2021). The future of phage biocontrol in integrated plant protection for sustainable crop production. Curr. Opin. Biotechnol. *68*, 60–71. https://doi.org/10.1016/j.copbio.2020.08.016.
7. Erdrich, S.H., Schurr, U., Frunzke, J., and Arsova, B. (2024). Seed coating with phages for sustainable plant biocontrol of plant pathogens and influence of the seed coat mucilage. Microb. Biotechnol. *17*, e14507. https://doi.org/10.1111/1751-7915.14507.
8. Salehimoghaddam, Z., Hynes, A.P., and Doyle, R.T. (2026). From bacterial predators to partners: phages in agriculture. New Phytol. *249*, 2729–2735. https://doi.org/10.1111/nph.70959.
9. Jones, J.D.G., and Dangl, J.L. (2006). The plant immune system. Nature *444*, 323–329. https://doi.org/10.1038/nature05286.
10. Abdul Malik, N.A., Kumar, I.S., and Nadarajah, K. (2020). Elicitor and Receptor Molecules: Orchestrators of Plant Defense and Immunity. Int. J. Mol. Sci. *21*, 963. https://doi.org/10.3390/ijms21030963.
11. Hussan, R.H., Dubery, I.A., and Piater, L.A. (2020). Identification of MAMP-Responsive Plasma Membrane-Associated Proteins in Arabidopsis thaliana Following Challenge with Different LPS Chemotypes from Xanthomonas campestris. Pathogens *9*, 787. https://doi.org/10.3390/pathogens9100787.
12. Offor, B.C., Mhlongo, M.I., Dubery, I.A., and Piater, L.A. (2022). Plasma Membrane-Associated Proteins Identified in Arabidopsis Wild Type, lbr2-2 and bak1-4 Mutants Treated with LPSs from Pseudomonas syringae and Xanthomonas campestris. Membranes *12*, 606. https://doi.org/10.3390/membranes12060606.
13. Aslam, S.N., Erbs, G., Morrissey, K.L., Newman, M.-A., Chinchilla, D., Boller, T., Molinaro, A., Jackson, R.W., and Cooper, R.M. (2009). Microbe-associated molecular pattern (MAMP) signatures, synergy, size and charge: influences on perception or mobility and host defence responses. Mol. Plant Pathol. *10*, 375–387. https://doi.org/10.1111/j.1364-3703.2009.00537.x.
14. Murakami, T., Katsuragi, Y., Hirai, H., Wataya, K., Kondo, M., and Che, F.-S. (2022). Distribution of flagellin CD2-1, flg22, and flgII-28 recognition systems in plant species and regulation of plant immune responses through these recognition systems. Biosci. Biotechnol. Biochem. *86*, 490–501. https://doi.org/10.1093/bbb/zbac007.
15. Gimenez-Ibanez, S., Ntoukakis, V., and Rathjen, J.P. (2009). The LysM receptor kinase CERK1 mediates bacterial perception in Arabidopsis. Plant Signal. Behav. *4*, 539–541. https://doi.org/10.4161/psb.4.6.8697.
16. Ma, X., Claus, L.A.N., Leslie, M.E., Tao, K., Wu, Z., Liu, J., Yu, X., Li, B., Zhou, J., Savatin, D.V., et al. (2020). Ligand-induced monoubiquitination of BIK1 regulates plant immunity. Nature *581*, 199–203. https://doi.org/10.1038/s41586-020-2210-3.
17. Lü, P., Liu, Y., Yu, X., Shi, C.-L., and Liu, X. (2022). The right microbe-associated molecular patterns for effective recognition by plants. Front. Microbiol. *13*, 1019069. https://doi.org/10.3389/fmicb.2022.1019069.
18. Boudsocq, M., Willmann, M.R., McCormack, M., Lee, H., Shan, L., He, P., Bush, J., Cheng, S.-H., and Sheen, J. (2010). Differential innate immune signalling via Ca2+ sensor protein kinases. Nature *464*, 418–422. https://doi.org/10.1038/nature08794.
19. Popescu, S.C., Popescu, G.V., Bachan, S., Zhang, Z., Gerstein, M., Snyder, M., and Dinesh-Kumar, S.P. (2009). MAPK target networks in *Arabidopsis thaliana* revealed using functional protein microarrays. Genes Dev. *23*, 80–92. https://doi.org/10.1101/gad.1740009.
20. Tena, G., Boudsocq, M., and Sheen, J. (2011). Protein kinase signaling networks in plant innate immunity. Curr. Opin. Plant Biol. *14*, 519–529. https://doi.org/10.1016/j.pbi.2011.05.006.
21. White, F.F., Potnis, N., Jones, J.B., and Koebnik, R. (2009). The type III effectors of *Xanthomonas*. Mol. Plant Pathol. *10*, 749–766. https://doi.org/10.1111/j.1364-3703.2009.00590.x.
22. Ryan, R.P., Vorhölter, F.-J., Potnis, N., Jones, J.B., Van Sluys, M.-A., Bogdanove, A.J., and Dow, J.M. (2011). Pathogenomics of Xanthomonas: understanding bacterium–plant interactions. Nat. Rev. Microbiol. *9*, 344–355. https://doi.org/10.1038/nrmicro2558.
23. Deslandes, L., and Rivas, S. (2012). Catch me if you can: bacterial effectors and plant targets. Trends Plant Sci. *17*, 644–655. https://doi.org/10.1016/j.tplants.2012.06.011.
24. Kazan, K., and Lyons, R. (2014). Intervention of Phytohormone Pathways by Pathogen Effectors. Plant Cell *26*, 2285–2309. https://doi.org/10.1105/tpc.114.125419.

25. Zhang, S., Li, C., Si, J., Han, Z., and Chen, D. (2022). Action Mechanisms of Effectors in Plant-Pathogen Interaction. Int. J. Mol. Sci. *23*, 6758. https://doi.org/10.3390/ijms23126758.

26. Büttner, D. (2016). Behind the lines–actions of bacterial type III effector proteins in plant cells. FEMS Microbiol. Rev. *40*, 894–937. https://doi.org/10.1093/femsre/fuw026.

27. Collier, S.M., and Moffett, P. (2009). NB-LRRs work a "bait and switch" on pathogens. Trends Plant Sci. *14*, 521–529. https://doi.org/10.1016/j.tplants.2009.08.001.

28. Dangl, J.L., and Jones, J.D. (2001). Plant pathogens and integrated defence responses to infection. Nature *411*, 826–833. https://doi.org/10.1038/35081161.

29. Thordal-Christensen, H. (2020). A holistic view on plant effector-triggered immunity presented as an iceberg model. Cell. Mol. Life Sci. *77*, 3963–3976. https://doi.org/10.1007/s00018-020-03515-w.

30. Rong, W., Feng, F., Zhou, J., and He, C. (2010). Effector-triggered innate immunity contributes *Arabidopsis* resistance to *Xanthomonas campestris*. Mol. Plant Pathol. *11*, 783–793. https://doi.org/10.1111/j.1364-3703.2010.00642.x.

31. Benjamin, G., Pandharikar, G., and Frendo, P. (2022). Salicylic Acid in Plant Symbioses: Beyond Plant Pathogen Interactions. Biology *11*, 861. https://doi.org/10.3390/biology11060861.

32. Okada, K., Abe, H., and Arimura, G.i. (2015). Jasmonates Induce Both Defense Responses and Communication in Monocotyledonous and Dicotyledonous Plants. Plant Cell Physiol. *56*, 16–27. https://doi.org/10.1093/pcp/pcu158.

33. Ruan, J., Zhou, Y., Zhou, M., Yan, J., Khurshid, M., Weng, W., Cheng, J., and Zhang, K. (2019). Jasmonic Acid Signaling Pathway in Plants. Int. J. Mol. Sci. *20*, 2479. https://doi.org/10.3390/ijms20102479.

34. Binder, B.M. (2020). Ethylene signaling in plants. J. Biol. Chem. *295*, 7710–7725. https://doi.org/10.1074/jbc.REV120.010854.

35. Chen, K., Li, G.J., Bressan, R.A., Song, C.P., Zhu, J.K., and Zhao, Y. (2020). Abscisic acid dynamics, signaling, and functions in plants. J. Integr. Plant Biol. *62*, 25–54. https://doi.org/10.1111/jipb.12899.

36. Kamle, M., Borah, R., Bora, H., Jaiswal, A.K., Singh, R.K., and Kumar, P. (2020). Systemic Acquired Resistance (SAR) and Induced Systemic Resistance (ISR): Role and Mechanism of Action Against Phytopathogens. In Fungal Biotechnology and Bioengineering Fungal Biology, A.E.-L. Hesham, R.S. Upadhyay, G.D. Sharma, C. Manoharachary, and V.K. Gupta, eds. (Springer International Publishing), pp. 457–470. https://doi.org/10.1007/978-3-030-41870-0_20.

37. Schikora, A., Schenk, S.T., and Hartmann, A. (2016). Beneficial effects of bacteria-plant communication based on quorum sensing molecules of theN-acyl homoserine lactone group. Plant Mol. Biol. *90*, 605–612. https://doi.org/10.1007/s11103-016-0457-8.

38. Vicente, J.G., and Holub, E.B. (2013). *Xanthomonas campestris* pv. *campestris* (cause of black rot of crucifers) in the genomic era is still a worldwide threat to brassica crops: *Xanthomonas campestris* pv. *campestris*. Mol. Plant Pathol. *14*, 2–18. https://doi.org/10.1111/j.1364-3703.2012.00833.x.

39. Dániel-Gómez, M., Reeves, E., and Meadows, I.M. (2022). Practical and Comprehensive Diagnostic Guide for Black Rot of Brassicas. Plant Health Prog. *23*, 369–375. https://doi.org/10.1094/PHP-08-21-0109-DG.

40. Roberts, S.J., Hiltunen, L.H., Hunter, P.J., and Brough, J. (1999). Transmission from Seed to Seedling and Secondary Spread of Xanthomonas campestris pv. Campestris in Brassica Transplants: Effects of Dose and Watering Regime. Eur. J. Plant Pathol. *105*, 879–889. https://doi.org/10.1023/A:1008790306489.

41. An, S.-Q., Potnis, N., Dow, M., Vorhölter, F.-J., He, Y.-Q., Becker, A., Teper, D., Li, Y., Wang, N., Bleris, L., and Tang, J.L. (2020). Mechanistic insights into host adaptation, virulence and epidemiology of the phytopathogen *Xanthomonas*. FEMS Microbiol. Rev. *44*, 1–32. https://doi.org/10.1093/femsre/fuz024.

42. Cerutti, A., Jauneau, A., Auriac, M.-C., Lauber, E., Martinez, Y., Chiarenza, S., Leonhardt, N., Berthomé, R., and Noël, L.D. (2017). Immunity at Cauliflower Hydathodes Controls Systemic Infection by *Xanthomonas campestris* pv *campestris*. Plant Physiol. *174*, 700–716. https://doi.org/10.1104/pp.16.01852.

43. Williams, P.H. (1980). Black Rot: A Continuing. Plant Dis. *64*, 736. https://doi.org/10.1094/PD-64-736.

44. He, Y.W., Boon, C., Zhou, L., and Zhang, L.H. (2009). Co-regulation of *Xanthomonas campestris* virulence by quorum sensing and a novel two-component regulatory system RavS/RavR. Mol. Microbiol. *71*, 1464–1476. https://doi.org/10.1111/j.1365-2958.2009.06617.x.

45. Erdrich, S.H., Sharma, V., Schurr, U., Arsova, B., and Frunzke, J. (2022). Isolation of Novel Xanthomonas Phages Infecting the Plant Pathogens X. translucens and X. campestris. Viruses *14*, 1449. https://doi.org/10.3390/v14071449.

46. Love, M.I., Huber, W., and Anders, S. (2014). Moderated estimation of fold change and dispersion for RNA-seq data with DESeq2. Genome Biol. *15*, 550. https://doi.org/10.1186/s13059-014-0550-8.

47. Nisar, N., Li, L., Lu, S., Khin, N.C., and Pogson, B.J. (2015). Carotenoid Metabolism in Plants. Mol. Plant *8*, 68–82. https://doi.org/10.1016/j.molp.2014.12.007.

48. Zhou, F., and Pichersky, E. (2020). More is better: the diversity of terpene metabolism in plants. Curr. Opin. Plant Biol. *55*, 1–10. https://doi.org/10.1016/j.pbi.2020.01.005.

49. Ninkuu, V., Zhang, L., Yan, J., Fu, Z., Yang, T., and Zeng, H. (2021). Biochemistry of Terpenes and Recent Advances in Plant Protection. Int. J. Mol. Sci. *22*, 5710. https://doi.org/10.3390/ijms22115710.

50. Vranová, E., Coman, D., and Gruissem, W. (2012). Structure and Dynamics of the Isoprenoid Pathway Network. Mol. Plant *5*, 318–333. https://doi.org/10.1093/mp/sss015.

51. Wang, Y., Pruitt, R.N., Nürnberger, T., and Wang, Y. (2022). Evasion of plant immunity by microbial pathogens. Nat. Rev. Microbiol. *20*, 449–464. https://doi.org/10.1038/s41579-022-00710-3.

52. Schwacke, R., Ponce-Soto, G.Y., Krause, K., Bolger, A.M., Arsova, B., Hallab, A., Gruden, K., Stitt, M., Bolger, M.E., and Usadel, B. (2019). MapMan4: A Refined Protein Classification and Annotation Framework Applicable to Multi-Omics Data Analysis. Mol. Plant *12*, 879–892. https://doi.org/10.1016/j.molp.2019.01.003.

53. Mao, J., Shen, B., Li, W., Liu, L., and Li, J. (2024). Post-translational Regulation of BRI1-EMS Suppressor 1 and Brassinazole-Resistant 1. Plant Cell Physiol. *65*, 1544–1551. https://doi.org/10.1093/pcp/pcae066.

54. Yang, Z., Guo, Z., Wang, S., An, Y., Fan, S., Jian, Y., Li, K., and Yi, Y. (2022). NAC062 acts as an upstream regulator of *NAC103* under endoplasmic reticulum stress. Agron. J. *114*, 1981–1994. https://doi.org/10.1002/agj2.20975.

55. Li, B., Fan, R., Guo, S., Wang, P., Zhu, X., Fan, Y., Chen, Y., He, K., Kumar, A., Shi, J., et al. (2019). The Arabidopsis MYB transcription factor, MYB111 modulates salt responses by regulating flavonoid biosynthesis. Environ. Exp. Bot. *166*, 103807. https://doi.org/10.1016/j.envexpbot.2019.103807.

56. Heyer, M., Scholz, S.S., Reichelt, M., Kunert, G., Oelmüller, R., and Mithöfer, A. (2022). The Ca2+ sensor proteins CML37 and CML42 antagonistically regulate plant stress responses by altering phytohormone signals. Plant Mol. Biol. *109*, 611–625. https://doi.org/10.1007/s11103-021-01184-2.

57. Rassizadeh, L., Cervero, R., Flors, V., and Gamir, J. (2021). Extracellular DNA as an elicitor of broad-spectrum resistance in Arabidopsis thaliana. Plant Sci. *312*, 111036. https://doi.org/10.1016/j.plantsci.2021.111036.

58. Scholz, S.S., Vadassery, J., Heyer, M., Reichelt, M., Bender, K.W., Snedden, W.A., Boland, W., and Mithöfer, A. (2014). Mutation of the Arabidopsis Calmodulin-Like Protein CML37 Deregulates the Jasmonate Pathway and Enhances Susceptibility to Herbivory. Mol. Plant *7*, 1712–1726. https://doi.org/10.1093/mp/ssu102.

59. Waidmann, S., Béziat, C., Ferreira Da Silva Santos, J., Feraru, E., Feraru, M.I., Sun, L., Noura, S., Boutté, Y., and Kleine-Vehn, J. (2023). Endoplasmic reticulum stress controls PIN-LIKES abundance and thereby growth adaptation. Proc. Natl. Acad. Sci. *120*, e2218865120. https://doi.org/10.1073/pnas.2218865120.

60. Glazebrook, J., Chen, W., Estes, B., Chang, H.S., Nawrath, C., Métraux, J.P., Zhu, T., and Katagiri, F. (2003). Topology of the network integrating salicylate and jasmonate signal transduction derived from global expression phenotyping. Plant J. *34*, 217–228. https://doi.org/10.1046/j.1365-313X.2003.01717.x.

61. Camoirano, A., Arce, A.L., Ariel, F.D., Alem, A.L., Gonzalez, D.H., and Viola, I.L. (2020). Class I TCP transcription factors regulate trichome branching and cuticle development in Arabidopsis. J. Exp. Bot. *71*, 5438–5453. https://doi.org/10.1093/jxb/eraa257.

62. Hayden, C.A., and Jorgensen, R.A. (2007). Identification of novel conserved peptide uORF homology groups in Arabidopsis and rice reveals ancient eukaryotic origin of select groups and preferential association with transcription factor-encoding genes. BMC Biol. *5*, 32. https://doi.org/10.1186/1741-7007-5-32.

63. Zhang, C., Lv, M., Yin, W., Dong, T., Chang, C., Miao, Y., Jia, Y., and Deng, Y. (2019). *Xanthomonas campestris* Promotes Diffusible Signal Factor Biosynthesis and Pathogenicity by Utilizing Glucose and Sucrose from Host Plants. Mol. Plant Microbe Interact. *32*, 157–166. https://doi.org/10.1094/MPMI-07-18-0187-R.

64. Oh, G.G.K., O'Leary, B.M., Signorelli, S., and Millar, A.H. (2022). Alternative oxidase (AOX) 1a and 1d limit proline-induced oxidative stress and aid salinity recovery in Arabidopsis. Plant Physiol. *188*, 1521–1536. https://doi.org/10.1093/plphys/kiab578.

65. Zhou, F., Emonet, A., Dénervaud Tendon, V., Marhavy, P., Wu, D., Lahaye, T., and Geldner, N. (2020). Co-incidence of Damage and Microbial Patterns Controls Localized Immune Responses in Roots. Cell *180*, 440–453.e18. https://doi.org/10.1016/j.cell.2020.01.013.

66. Poncini, L., Wyrsch, I., Dénervaud Tendon, V., Vorley, T., Boller, T., Geldner, N., Métraux, J.-P., and Lehmann, S. (2017). In roots of Arabidopsis thaliana, the damage-associated molecular pattern AtPep1 is a stronger elicitor of immune signalling than flg22 or the chitin heptamer. PLoS One *12*, e0185808. https://doi.org/10.1371/journal.pone.0185808.

67. Büttner, D., and Bonas, U. (2010). Regulation and secretion of *Xanthomonas* virulence factors. FEMS Microbiol. Rev. *34*, 107–133. https://doi.org/10.1111/j.1574-6976.2009.00192.x.

68. Tondo, M.L., Delprato, M.L., Kraiselburd, I., Fernández Zenoff, M.V., Farías, M.E., and Orellano, E.G. (2016). KatG, the Bifunctional Catalase of Xanthomonas citri subsp. citri, Responds to Hydrogen Peroxide and Contributes to Epiphytic Survival on Citrus Leaves. PLoS One *11*, e0151657. https://doi.org/10.1371/journal.pone.0151657.

69. Gao, L., Altae-Tran, H., Böhning, F., Makarova, K.S., Segel, M., Schmid-Burgk, J.L., Koob, J., Wolf, Y.I., Koonin, E.V., and Zhang, F. (2020). Diverse enzymatic activities mediate antiviral immunity in prokaryotes. Science *369*, 1077–1084. https://doi.org/10.1126/science.aba0372.

70. Yamoune, A., Zdarska, M., Depaepe, T., Rudolfova, A., Skalak, J., Berendzen, K.W., Mira-Rodado, V., Fitz, M., Pekarova, B., Nicolas Mala, K.L., et al. (2024). Cytokinins regulate spatially specific ethylene production to control root growth in Arabidopsis. Plant Commun. *5*, 101013. https://doi.org/10.1016/j.xplc.2024.101013.

71. Yang, W., Cortijo, S., Korsbo, N., Roszak, P., Schiessl, K., Gurzadyan, A., Wightman, R., Jönsson, H., and Meyerowitz, E. (2021). Molecular mechanism of cytokinin-activated cell division in *Arabidopsis*. Science *371*, 1350–1355. https://doi.org/10.1126/science.abe2305.

72. Holtappels, D., Fortuna, K.J., Moons, L., Broeckaert, N., Bäcker, L.E., Venneman, S., Rombouts, S., Lippens, L., Baeyen, S., Pollet, S., et al. (2022). The potential of bacteriophages to control *Xanthomonas campestris* pv. *campestris* at different stages of disease development. Microb. Biotechnol. *15*, 1762–1782. https://doi.org/10.1111/1751-7915.14004.

73. Nakayinga, R., Makumi, A., Tumuhaise, V., and Tinzaara, W. (2021). Xanthomonas bacteriophages: a review of their biology and biocontrol applications in agriculture. BMC Microbiol. *21*, 291. https://doi.org/10.1186/s12866-021-02351-7.

74. Hernandez, C.A., Delesalle, V.A., Krukonis, G.P., DeCurzio, J.M., and Koskella, B. (2024). Genomic and phenotypic signatures of bacteriophage coevolution with the phytopathogen *Pseudomonas syringae*. Mol. Ecol. *33*, e16850. https://doi.org/10.1111/mec.16850.

75. Hernandez, C.A., and Koskella, B. (2019). Phage resistance evolution *in vitro* is not reflective of *in vivo* outcome in a plant-bacteria-phage system. Evolution *73*, 2461–2475. https://doi.org/10.1111/evo.13833.

76. Fortuna, K.J., Holtappels, D., Venneman, J., Baeyen, S., Vallino, M., Verwilt, P., Rediers, H., De Coninck, B., Maes, M., Van Vaerenbergh, J., et al. (2023). Back to the Roots: *Agrobacterium* -Specific Phages Show Potential to Disinfect Nutrient Solution from Hydroponic Greenhouses. Appl. Environ. Microbiol. *89*, e00215-23. https://doi.org/10.1128/aem.00215-23.

77. Vu, N.T., Kim, H., Hwang, I.S., and Oh, C.-S. (2025). Colanic acid and lipopolysaccharide in Pectobacterium carotovorum Pcc21 serve as receptors for the bacteriophage phiPccP-2. Microbiol. Res. *290*, 127939. https://doi.org/10.1016/j.micres.2024.127939.

78. Supina, B.S.I., McCutcheon, J.G., Peskett, S.R., Stothard, P., and Dennis, J.J. (2025). A flagella-dependent *Burkholderia* jumbo phage controls rice seedling rot and steers *Burkholderia glumae* toward reduced virulence in rice seedlings. mBio *16*, e0281424. https://doi.org/10.1128/mbio.02814-24.

79. Alvarez-Martinez, C.E., Sgro, G.G., Araujo, G.G., Paiva, M.R.N., Matsuyama, B.Y., Guzzo, C.R., Andrade, M.O., and Farah, C.S. (2021). Secrete or perish: The role of secretion systems in Xanthomonas biology. Comput. Struct. Biotechnol. J. *19*, 279–302. https://doi.org/10.1016/j.csbj.2020.12.020.

80. Teper, D., Pandey, S.S., and Wang, N. (2021). The HrpG/HrpX Regulon of Xanthomonads—An Insight to the Complexity of Regulation of Virulence Traits in Phytopathogenic Bacteria. Microorganisms *9*, 187. https://doi.org/10.3390/microorganisms9010187.

81. Nivaskumar, M., and Francetic, O. (2014). Type II secretion system: A magic beanstalk or a protein escalator. Biochim. Biophys. Acta *1843*, 1568–1577. https://doi.org/10.1016/j.bbamcr.2013.12.020.

82. Timilsina, S., Potnis, N., Newberry, E.A., Liyanapathiranage, P., Iruegas-Bocardo, F., White, F.F., Goss, E.M., and Jones, J.B. (2020). Xanthomonas diversity, virulence and plant–pathogen interactions. Nat. Rev. Microbiol. *18*, 415–427. https://doi.org/10.1038/s41579-020-0361-8.

83. Van Belleghem, J.D., Dąbrowska, K., Vaneechoutte, M., Barr, J.J., and Bollyky, P.L. (2018). Interactions between Bacteriophage, Bacteria, and the Mammalian Immune System. Viruses *11*, 10. https://doi.org/10.3390/v11010010.

84. Barr, J.J., Auro, R., Furlan, M., Whiteson, K.L., Erb, M.L., Pogliano, J., Stotland, A., Wolkowicz, R., Cutting, A.S., Doran, K.S., et al. (2013). Bacteriophage adhering to mucus provide a non–host-derived immunity. Proc. Natl. Acad. Sci. *110*, 10771–10776. https://doi.org/10.1073/pnas.1305923110.

85. Chin, W.H., Kett, C., Cooper, O., Müseler, D., Zhang, Y., Bamert, R.S., Patwa, R., Woods, L.C., Devendran, C., Korneev, D., et al. (2022). Bacteriophages evolve enhanced persistence to a mucosal surface. Proc. Natl. Acad. Sci. *119*, e2116197119. https://doi.org/10.1073/pnas.2116197119.

86. You, X., Kallies, R., Kühn, I., Schmidt, M., Harms, H., Chatzinotas, A., and Wick, L.Y. (2022). Phage co-transport with hyphal-riding bacteria fuels bacterial invasion in a water-unsaturated microbial model system. ISME J. *16*, 1275–1283. https://doi.org/10.1038/s41396-021-01155-x.

87. Kolozsváriné Nagy, J., Schwarczinger, I., Künstler, A., Pogány, M., and Király, L. (2015). Penetration and translocation of Erwinia amylovora-specific bacteriophages in apple - a possibility of enhanced control of fire blight. Eur. J. Plant Pathol. *142*, 815–827. https://doi.org/10.1007/s10658-015-0654-3.

88. Rahimi-Midani, A., and Choi, T.-J. (2020). Transport of Phage in Melon Plants and Inhibition of Progression of Bacterial Fruit Blotch. Viruses *12*, 477. https://doi.org/10.3390/v12040477.

89. Zang, Z., Zhang, C., Park, K.J., Schwartz, D.A., Podicheti, R., Lennon, J.T., and Gerdt, J.P. (2025). Streptomyces secretes a siderophore that sensitizes competitor bacteria to phage infection. Nat. Microbiol. *10*, 362–373. https://doi.org/10.1038/s41564-024-01910-8.

90. Moser, R., Aktas, M., and Narberhaus, F. (2014). Phosphatidylcholine biosynthesis in *X anthomonas campestris* via a yeast-like acylation pathway: Methylated phospholipids in *Xanthomonas*. Mol. Microbiol. *91*, 736–750. https://doi.org/10.1111/mmi.12492.

91. Schindelin, J., Arganda-Carreras, I., Frise, E., Kaynig, V., Longair, M., Pietzsch, T., Preibisch, S., Rueden, C., Saalfeld, S., Schmid, B., et al. (2012). Fiji: an open-source platform for biological-image analysis. Nat. Methods *9*, 676–682. https://doi.org/10.1038/nmeth.2019.

92. Bolger, A.M., Lohse, M., and Usadel, B. (2014). Trimmomatic: a flexible trimmer for Illumina sequence data. Bioinformatics *30*, 2114–2120. https://doi.org/10.1093/bioinformatics/btu170.

93. Murashige, T., and Skoog, F. (1962). A Revised Medium for Rapid Growth and Bio Assays with Tobacco Tissue Cultures. Physiol. Plant. *15*, 473–497. https://doi.org/10.1111/j.1399-3054.1962.tb08052.x.

94. M.R.J. Clokie and A.M. Kropinski, eds. (2009). Bacteriophages (Humana Press). https://doi.org/10.1007/978-1-60327-164-6.

95. Korniienko, N., Kharina, A., Zrelovs, N., Jindřichová, B., Moravec, T., Budzanivska, I., Burketová, L., and Kalachova, T. (2022). Isolation and Characterization of Two Lytic Phages Efficient Against Phytopathogenic Bacteria From Pseudomonas and Xanthomonas Genera. Front. Microbiol. *13*, 853593. https://doi.org/10.3389/fmicb.2022.853593.

96. Rhee, S.Y., Beavis, W., Berardini, T.Z., Chen, G., Dixon, D., Doyle, A., Garcia-Hernandez, M., Huala, E., Lander, G., Montoya, M., et al. (2003). The Arabidopsis Information Resource (TAIR): a model organism database providing a centralized, curated gateway to Arabidopsis biology, research materials and community. Nucleic Acids Res. *31*, 224–228. https://doi.org/10.1093/nar/gkg076.

97. Bray, N.L., Pimentel, H., Melsted, P., and Pachter, L. (2016). Near-optimal probabilistic RNA-seq quantification. Nat. Biotechnol. *34*, 525–527. https://doi.org/10.1038/nbt.3519.

98. Marhavý, P., Kurenda, A., Siddique, S., Dénervaud Tendon, V., Zhou, F., Holbein, J., Hasan, M.S., Grundler, F.M., Farmer, E.E., and Geldner, N. (2019). Single-cell damage elicits regional, nematode-restricting ethylene responses in roots. EMBO J. *38*, e100972. https://doi.org/10.15252/embj.2018100972.

99. Juszczak, I., and Baier, M. (2014). Quantification of Superoxide and Hydrogen Peroxide in Leaves. In Plant Cold Acclimation Methods in Molecular Biology, D.K. Hincha and E. Zuther, eds. (Springer), pp. 217–224. https://doi.org/10.1007/978-1-4939-0844-8_16.

100. Rao, X., Huang, X., Zhou, Z., and Lin, X. (2013). An improvement of the 2 ^(-delta delta CT) method for quantitative real-time polymerase chain reaction data analysis. Biostat. Bioinforma. Biomath. *3*, 71–85.

STAR★METHODS

KEY RESOURCES TABLE

REAGENT or RESOURCE	SOURCE	IDENTIFIER
Bacterial and virus strains		
Xanthomonas campestris pv. *Campestris* 8004	AG Narberhaus (RUB, Bochum)[90]	DSM 118660
Xanthomonas campestris pv. *Campestris* Δ XC_4244	This study	–
Xanthomonas phage Seregon	Erdrich et al. 2022[45]	NCBI: ON189048
Chemicals, peptides, and recombinant proteins		
3,3′-diaminobenzidine (DAB)	Thermo Fisher Scientific	Cat no. H54000.14
Critical commercial assays		
Rneasy® Plant Mini Kit	Qiagen	Cat no./ID. 74904
DNAse I	Thermo Fisher Scientific	Cat no. AM1906
SuperScript IV reverse transcriptase	Thermo Fisher Scientific	Cat no. 18090050
iQ SYBR Green Supermix	Bio-Rad	Cat no. #1708880
Deposited data		
Raw and analyzed RNA Seq data	This Paper	GEO: GSE294853
Experimental models: Organisms/strains		
Arabidopsis thaliana Col-0 pAOS::NLS-3xVenus	Poncini et al. 2019[66]	N/A
Arabidopsis thaliana Col-0 pPER5:NLS-3xVenus	Poncini et al. 2019[66]	N/A
Oligonucleotides		
Table S8	This study	N/A
Software and algorithms		
ImageJ (Version 1.54f)	Schindelin et al. 2012[91]	https://imagej.net/
Nikon NIS Elements 4.0 software	Nikon	https://www.microscope.healthcare.nikon.com/en_EU/products/software/nis-elements
FastQC software v.0.11.9	Babraham Institute	http://www.bioinformatics.babraham.ac.uk/projects/fastqc/
Trimmomatic tool v. 0.39	Bolger et al. 2014[92]	http://www.usadellab.org/cms/?page=trimmomatic
DESeq2 Algorithm	R (v4.2.2)	N/A

EXPERIMENTAL MODEL

Plant propagation

Arabidopsis thaliana Col-0 plants were propagated on ½ Murashige and Skoog-Agar (½ MS).[93] Individual surface sterilized seeds (70% EtOH +0.01% Triton X- for 3 min, 99% EtOH for 15 s, air dried on sterile filter paper under a laminar flow bench) were placed in a Petri dish in a 3x3 matrix under a laminar flow bench. Plates were sealed with micropore tape (3M micropore tape, 3M Deutschland GmbH) and put into a climate chamber (CLF Plant Climatics GmbH, SED41-CU4C2LT or Percival Scientific, Model AR-22L) with a 12 h light–12 h dark regime at 22°C day and 18°C night, with 100 μE illumination at a relative humidity of 60%. At the start of the experiment, each condition contained 216 plants.

Bacterial growth conditions

Xanthomonas campestris pv. campestris str. 8004, featured in several studies and derived from a natural *Xcc* isolate obtained from Cauliflower in the UK 1958,[38] was used in this study. Bacteria were grown on nutrient agar (5.0 g peptone, 3.0 g yeast extract and 15.0 g Agar in 1,000 mL of dH_2O). Liquid cultures were inoculated from single colonies and propagated in nutrient broth

(5.0 g peptone, 3.0 g yeast extract in 1,000 mL of dH_2O) overnight. Unless mentioned otherwise, bacterial cultivation was performed in shake flasks at 28°C and 150 rpm.

Phage amplification

The *Xanthomonas* phage Seregon (GenBank: ON189048) was isolated and described previously,[45] briefly a lytic bacteriophage with a siphovirion morphology specific to *Xcc* str. 8004, isolated from a waste water sample. Phages were either amplified on plates or in liquid cultures. For plate amplification, a double agar overlay[94] was prepared using 100 μL phage solution with a titer 10^8 plaque-forming units (pfu) ml^{-1} added to 3.5 mL 0.4%-top agar containing the bacterium at a final OD_{600} of 0.2. Harvesting of purified phage particles was performed after overnight incubation. The top agar was solubilized by adding 3 mL ½ MS liquid medium followed by two hours of incubation on a rock shaker. The solution was subsequently transferred into a falcon tube and centrifuged at 5000 *g* for 25 min to remove residual amounts of agar and bacterial cell fragments. The supernatant was filtered twice through 0.2 μM syringe filters and stored at 4°C. For titer determination, a dilution series was spotted on overlay agar, and the visible plaques at the highest dilution were counted to determine the plaque-forming units per mL.

METHOD DETAILS

Plant inoculation

Plant inoculation was performed using a flood-inoculation method adapted from Korniienko et al.2021.[95] Eight-day-old seedlings were inoculated by flooding each plate with 50 mL of ½ MS liquid medium containing 1×10^9 cfu mL^{-1} of *Xcc* for the pathogen-only and pathogen-plus-phage treatments. To prepare inocula, both the bacterial culture and the phage stock were first purified by centrifugation and resuspended in ½ MS medium. Concentrated stocks were then diluted into the 50 mL inoculation solution to obtain the required final concentrations.

For the phage treatment, phages were added directly to the *Xcc* inoculum immediately before flooding to achieve a multiplicity of infection of 5 (*Xcc*+ ϕ MOI5 = five phages per bacterial cell). The phage-only control received 50 mL of ½ MS containing the same final phage concentration used in the *Xcc*+ ϕ MOI 5 treatment but without bacteria. The plant-only control was flooded with 50 mL of ½ MS medium.

Seedlings were submerged for 5 min, after which the inoculation medium was carefully removed. Plates were then sealed with micropore tape and returned to the climate chamber. Plant growth under all treatment conditions was consistent across five independent experimental rounds, and all biological samples used for downstream analyses were collected in triplicate.

Non-invasive plant phenotyping

The non-invasive plant phenotyping was performed at 0, 2, 5, 7, 9 and 14 days post-infection (dpi). Plates were placed onto an Epson 10000XL WinRhizo scanner, and images were acquired using the manufacturer's scanner interface. The top of the plates was covered with white cardboard for better contrast. Tiff images were retrieved by scanning from below, with a resolution of 1200 dpi.

Invasive plant phenotyping and extraction of microbes

The invasive plant phenotyping was performed in a separate experiment and plants were harvested at 0, 2, 5, 7 and 14 (dpi). The fresh weight of plants was determined by placing plants into pre-weighed microcentrifuge tubes containing one 3 mm glass beads using sterile tweezers. For the duration of the experiment, samples were kept on ice. The fresh weight was determined by subtracting the pre-weighed weight of the tube including the glass bead-weight from the final weight.

For bacterial cfu and phage pfu determination 1 mL of ½ MS media was added to the fresh weight and the tissue was disrupted by using a ball mill for 10s at 60Hz/s. Afterward, a dilution series was prepared for each sample. To determine the bacterial load 3 μL of each dilution step were plated on NB-Agar plates containing rifampicin and cfu's was determined after 48 h incubation at 28°C. To determine the amount of infectious phage particles pfu ml^{-1}, a double agar overlay was prepared as described above and 3μL of each dilution step were plated on top. Phage titer was determined after 24 h incubation at 28°C.

RNA extraction

For RNA extraction, multiple plants with a total weight of 45 mg were harvested from each treatment group and pooled in a micro-centrifuge tube. The obtained tissue was immediately frozen in liquid nitrogen and stored at −80°C. Sampling occurred in triplicates at 0, 2 and 7 dpi. For nucleic acid extraction, the frozen tissue was ground in a ball mill (Retsch MM200, Retsch, Germany) with a 4–5 mm stainless steel beat. Total RNA extraction from the resulting tissue powder was performed using the Rneasy Plant Mini Kit (Qiagen, Hilden, Germany) according to the manufacturer's instructions. To remove genomic DNA contamination, total RNA was incubated with DNAse I (Thermo Fisher Scientific, AM1906) for 15 min.

RNA-seq

At the start of the experiment, each condition contained 216 plants; the plants for RNA extraction were harvested throughout the experiment at 0, 2, and 7 days post-inoculation. RNA-Seq was performed for samples of the conditions: control, phage only, *Xcc* and XCC+ Φ at 2 and 7 dpi, each in three biological replicates as well as one triplicate of plants directly before treatment (0 dpi)

was performed with rRNA depletion strand-specific RNA library preparation at Azenta Life Science, followed by RNA-Seq on a Novaseq 6,000 with a sequencing depth of 100M read pairs per sample (2x 150 bp). Raw read sequences were archived at NCBI (GSE294853). The read quality was assessed with the FastQC software v.0.11.9 (http://www.bioinformatics.babraham.ac.uk/projects/fastqc/). Sequencing adapters and low-quality sequences were removed using the Trimmomatic tool v. 0.39.[92] The obtained reads were mapped against the *Arabidopsis thaliana* genome (TAIR 10.0)[96] using Kallisto.[97] Genome mapping against the other species (*Xcc* [NC_007086.1] and phage Seregon [ON189048.1]) was performed in subsequent rounds using Kallisto.

Imaging of nuclear reporter lines

For microscopic analysis of pAOS::NLS-3xVenus and pPER5:NLS-3xVenus reporter lines[98] seven-day-old seedlings were carefully transferred onto ½ MS agar medium flood inoculated as described above with *Xcc*, phage Seregon, or XCC+ Φ solution, and grown for 48 h prior to imaging. The seedlings were observed under spinning-disk confocal microscope 48 h post inoculation.

Imaging of plant roots was done using a custom-build fluorescent microscope with a Nikon Ti-E stand, equipped with a Nikon 10× objective (S Fluor, N.A. = 0.50), CrestOptics X-light spinning disk (pinhole size 50μm), motorized stage (Applied Scientific Instrumentation, USA), motorized filter wheel (Cairn Research, UK), laser launch (Omicron, Germany), dichroic mirror (Chroma triple band 440/514/561), and an sCMOS camera (Teledyne Photometrics, Prime 95B, USA). Image acquisition was operated through Nikon NIS Elements 4.0 software. Imaging of reporter lines and PI staining were done with 520nm excitation (80mW power), with a 542/20 emission filter for reporter lines, and 605/70 emission filter for PI staining.

Histochemical staining of reactive oxygen species

For semiquantitative analysis of hydrogen peroxide (H_2O_2) levels in plant tissue, histochemical staining utilizing 3,3′-diaminobenzidine (DAB), was conducted, as described previously,[99] with modifications as described below. Staining was carried out all conditions at 0, 2, 7 and 14 dpi, as described in 2.4. For each condition and time point, 5 to 10 plants were used for staining. DAB-staining solution was prepared by dissolving DAB in phosphate-buffered saline solution (PBS; 8 g sodium chloride, 0.2 g potassium chloride, 1.44 g disodium hydrogen phosphate, and 0.24 g potassium dihydrogen phosphate in 1,000 mL of dH_2O at pH 7.4), to a concentration of 0.1 mg per mL, then wrapped in aluminum foil to minimize degradation of light sensitive components. The DAB-staining solution was sterile filtered using a Filtropur S (Sarstedt, Germany) syringe filter with 0.2 μm pore size, then transferred to flat base 6 well cell culture plates (Sarstedt, Germany), adding 5 mL per well. After non-invasive phenotyping plants were carefully taken from the respective plates with spring steel tweezers and transferred to the prepared staining solution. The plates were closed and wrapped in aluminum foil, then transferred to a desiccator with attached vacuum pump (MZ 2C, vacuubrand, Germany). To improve tissue penetration of the staining solution, vacuum evacuation was conducted in three rounds of 5 min each. Subsequent incubation in darkness at RT and ambient pressure was performed for 24 h. After incubation, the DAB-staining solution was removed and prewarmed (60°C) destaining solution (100 mL concentrated acetic acid, 100 mL glycerol, 300 mL 96% ethanol mixed for 500 mL destaining solution) was added to the wells containing plants, to get rid of chlorophylls and other pigments. To aid in this process, a water bath set to 60°C (Hydro H 8, Lauda, Germany) in contact with the bottom of the flat bases of the wells, was used to add heat during the destaining. The destaining solution was replaced, till no further chlorophyll could be extracted, indicated by a translucent appearance of the unstained plant tissue. Subsequently, the plants were transferred between two sheets of clear film, using spring steel tweezers, making sure to remove any excess liquid, and placing the leaves without overlap. The plants were scanned using Epson 10000XL WinRhizo scanner.

RT-qPCR

For quantitative real-time PCR, cDNA was synthesized using 1000 ng of total RNA. First-strand cDNA was synthesized using SuperScript IV reverse transcriptase (Thermo Fisher Scientific, cat. no. 18090050). For quantitative real-time PCR, 50 ng first-strand cDNA in 2 μL was mixed with 0.6 μL of 10 μM solution of the oligonucleotide pair of interest, together with 10 μL iQ SYBR Green Supermix (Bio-Rad) and water to a total volume of 20 μL. The PCR was performed using a qPCR Bio-Rad CFX Connect system employing the following program: 95°C for 2 min, followed by 35 cycles of 95°C for 10 s, 55°C for 10 s, and 72°C for 20 s. The oligonucleotides used for the genes of interest are listed in Supplementary Table S8. The ΔCq and ΔΔCq values were calculated as described in.[100]

QUANTIFICATION AND STATISTICAL ANALYSIS

Quantification of green area during non-invasive plant phenotyping

The plant leaf area was calculated using ImageJ (Version 1.54f), and green pixels were isolated by HSV thresholding. The leaf area of each plant was determined using the ‘‘analyze particle’’ function. Data were analyzed using ANOVA test followed by Tukey HSD, shown as Compact Letter Display (CLD). Details can be found in Figure 1.

Differential expression analysis of RNA-Seq

Differential expression analysis was performed using DESeq2.[46] The DESeq2 Algorithm attained the differentially expressed genes using the Wald test and DEGs were corrected for multiple testing using the Benjamini and Hochberg method. The significance cut off were set to <0.05 p-adj and LogFC >1. All details, including padj values can be found in Supplemental Table 6 (Raw DEGs.xlsx).

Quantification of images of nuclear reporter lines

After acquisition, the data were processed and analyzed with ImageJ/Fiji (version 1.49b), following the "Subtract background" (rolling ball radius = 200px) function, and the "Gaussian Blur" (sigma = 1 radius) filter. Maximum intensity projections were generated for each dataset. At least two independent experiments were performed, with 6–12 replicates analyzed. Sample numbers AOS: Mock 13; Seregon 13; Xcc 22; XCC+ Φ 26. PER5: Mock, Seregon, Xcc, XCC+ Φ = 7.

Data were analyzed with non-parametric test, due to nonnormal distribution and unequal variances. Overall group differences were assessed using the Kruskal–Wallis rank-sum test (stats package), followed by pairwise comparisons with Dunn's test (FSA package, v0.9.4) and Benjamini–Hochberg correction. Significance groupings were visualized using compact letter displays from the multcompView package (v0.1-9), Figure 4.

Quantification of histochemical staining of reactive oxygen species

Scanned plant leaves were analyzed using ImageJ (Version 1.54f), with the inverted average gray value, indicating staining intensity. ANOVA test followed by Tukey HSD $F = 75.8$, $p = 6.26e{-}75$, with significant differences marked by different letters using Compact Letter Display (CLD). For more details see supplemental figures S4 and S5.

Statistical analysis of qRT-PCR results of plant and bacterial transcripts

Quantification of plant and bacterial transcripts ($2\text{-}\Delta\Delta Ct$) is calculated compared to Xcc in both cases. Error bars represent ± SD; $n = 3$. Significant differences (*) are shown after a pairwise comparison using Student's t test, always for one transcript and time point, Figure S3.